Journal of Nanobiotechnology

RESEARCH

Open Access

# Photo-controlled co-delivery of verteporfin and acriflavine via platelets achieves potentiated glioblastoma-targeted photodynamic therapy

Jie Guo[1†], Meng-Fei Wang[1,2†], Shen-Jun Yuan[3†], Ke Li[4], Quan Zhang[5], Hui-Mei Lei[1], Jia-Lin Wu[1], An-Xin Li[1], Yong-Hong Xu[6*] and Xiao Chen[1,7*]

## Abstract

The potential of glioblastoma (GBM) photodynamic therapy (PDT) is limited by inadequate GBM drug delivery, and the development of resistance to PDT as a result of cellular damage response that critically involves the hypoxia-inducible factor-1α (HIF-1α) and yes-associated protein (YAP). Herein, addressing these challenges, we demonstrated a strategy of photo-controlled, targeted co-delivery of verteporfin (Vp), a photosensitizer and YAP inhibitor as well, and acriflavine (Af), a HIF-1α inhibitor via platelets for enhanced GBM PDT. Mouse platelets were separately loaded with Vp (Vp@Plt) and Af (Af@Plt) and the mixture thereof is termed Vp@Plt + Af@Plt. Alternatively, platelets were simultaneously loaded with Vp and Af to yield (Vp + Af)@Plt. First, both Vp@Plt + Af@Plt and (Vp + Af)@Plt were shown to achieve rapid and efficient laser-triggered, GBM-targeted delivery of Vp and Af, which led to markedly higher phototoxicity in the GBM cells (GBCs) and ultimately more potent GBM PDT than Vp@Plt in mice. Next, a mechanistic study revealed the induction of a mutually promotional interaction of HIF-1α and YAP in the GBCs in response to PDT-inflicted DNA damage. This interaction protected HIF-1α from degradation and meanwhile assisted in the nuclear translocation of YAP leading to increased nuclear presence of both HIF-1α and YAP and escalated DNA damage repair activity under their regulation. Both Af and Vp were found to block the PDT-induced HIF-1α-YAP interaction and thereby severely impaired DNA damage repair, eventually resulting in exacerbated cell death. In conclusion, Af and Vp can be adequately co-delivered in GBM via platelets in a photo-controlled manner to achieve efficacious GBM PDT through double blocking of the HIF-1α-YAP interaction in the GBCs.

†Jie Guo, Meng-Fei Wang and Shen-Jun Yuan contributed equally to this work.

*Correspondence:
Yong-Hong Xu
2420749884@qq.com
Xiao Chen
chen-xiao@whu.edu.cn

Full list of author information is available at the end of the article

**Graphical abstract**

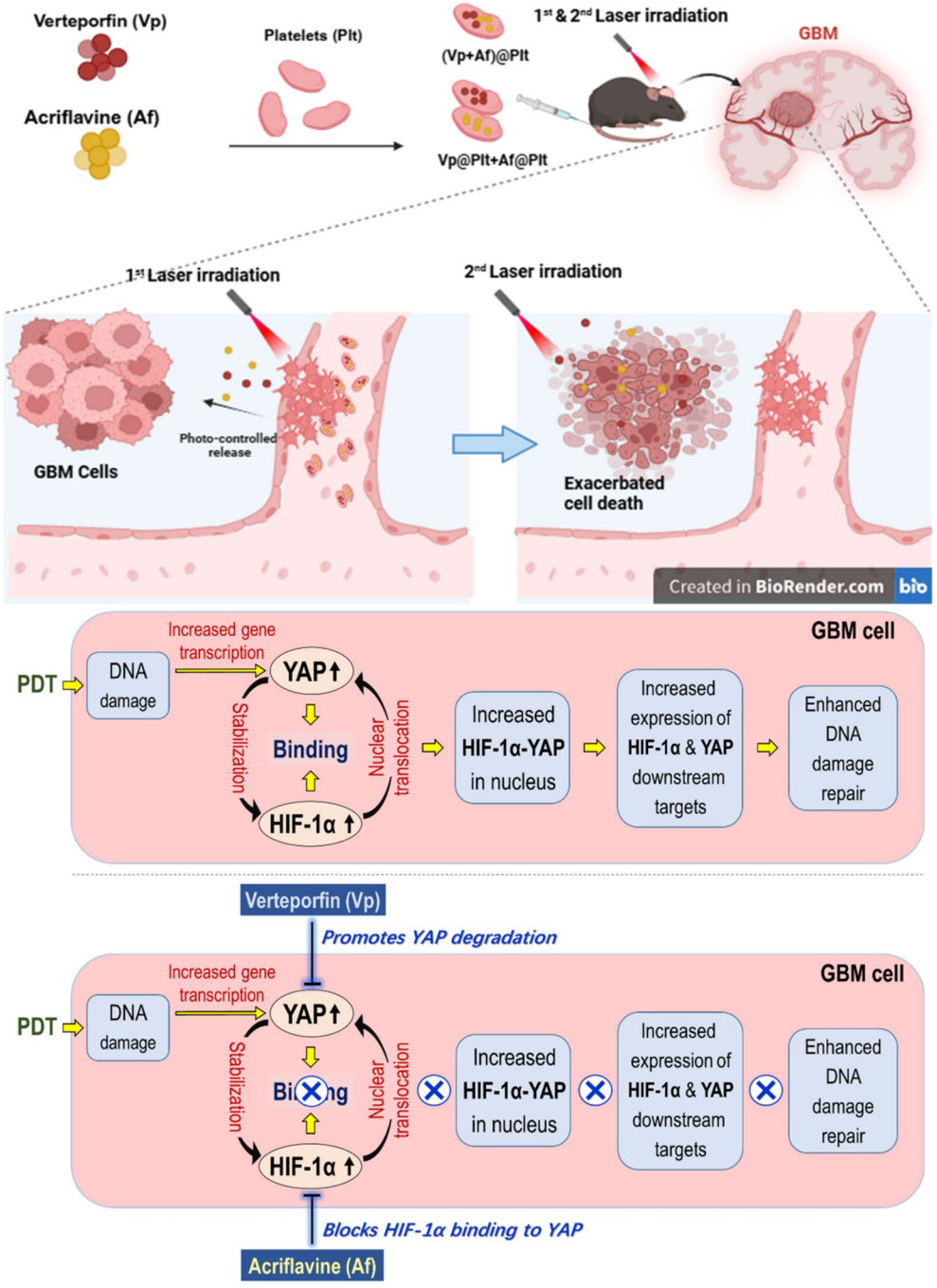


**Keywords** Glioblastoma, Platelets, Acriflavine, HIF-1α, Verteporfin, YAP

## Introduction

Glioblastoma (GBM) is a highly aggressive type of brain tumor classified as a grade IV astrocytoma that originates from astrocytes in the brain and spinal cord [1]. GBM is the most common high-grade primary brain tumor in adults and is characterized by rapid growth and a tendency to invade nearby brain tissue, making it one of the most lethal types of brain cancer [2, 3]. GBM can result in death within six months or less without treatment. Even with treatment, the prognosis remains poor due to GBM's resistance to conventional therapies and the brain's limited capacity to repair itself. Currently,

the treatment of GBM involves a multi-modal approach aiming to extend survival and improve quality of life, although a cure remains elusive [2–4]. The standard care of GBM involves maximal safe surgical resection to reduce its size and alleviate symptoms followed by concurrent chemoradiotherapy and adjuvant temozolomide (TMZ) to target residual tumor cells and further control tumor growth [5, 6]. This approach, however, has not significantly improved survival rates, which remain low, with a median survival of approximately 8 to 15 months post-diagnosis. This predicament largely stems from some difficult challenges in the treatment of GBM, such as the GBM cells' (GBCs') inherent resistance to many conventional therapies and the blood-brain barrier and disrupted tumor blood supply which hinder effective drug delivery to the tumor site. Recurrence is common despite aggressive treatment, and the tumor often returns more resistant to treatment [7, 8]. Given the situation, there is an imperative need for innovative therapeutic strategies and approaches. Emerging therapies, such as photodynamic therapy (PDT), are being intensely investigated for the treatment of GBM.

PDT works by sensitizing tumor tissue with a photosensitizer, followed by exposure to a specific wavelength of light to activate the photosensitizer. The energized photosensitizer then converts molecular oxygen in the milieu into highly reactive oxygen species (ROS), particularly singlet oxygen, which induces cell damage and death [9–12]. PDT also disrupts the blood vessels supplying the tumor, depriving it of necessary nutrients and oxygen, which leads to tumor cell death [13]. There are reports that PDT can stimulate anti-tumor immune responses [13–15]. PDT offers a highly targeted, minimally invasive, and effective treatment option for GBM, with the added benefits of fewer side effects and the potential to overcome resistance to conventional therapies [15–18]. Recent developments indicate that PDT may enhance local control of tumors and improve patient outcomes, particularly when combined with standard therapies like surgery, chemotherapy, and radiotherapy [19–23]. Despite its great potential, PDT faces several challenges that severely limit translation of its value in the treatment of GBM, the most salient among which are inadequate tumor photosensitizer distribution and retention and development of resistance [17, 19, 23, 24].

In this study, we propose to overcome the two challenges at the same time using a strategy of 'GBM-targeted co-delivery of verteporfin (Vp) and acriflavine (Af)', which is explained below. Vp is a benzoporphyrin derivative photosensitizer that can be excited by 690 nm of laser and has been clinically used for PDT of the wet form of macular degeneration [25]. Af is an acridine derivative with pleitropic biological effects, but best known for its inhibition of the hypoxia-inducible factor-1α (HIF-1α) [26]. HIF-1α is a subunit of a heterodimeric transcription factor hypoxia-inducible factor 1 (HIF-1) and is considered the master transcriptional regulator of cellular and developmental response to hypoxia [27–29]. HIF-1α is also critically involved in the cellular damage responses, which underlie the development of tumor resistance to multiple therapies [30–35]. In a preliminary study, we performed RNA sequencing analysis of in vitro mouse GBCs exposed to Vp under 690 nm laser irradiation (LI). Obtained results revealed upregulated genes that are mostly related to cellular responses to decreased oxygen levels, hypoxia, and the HIF-1 signaling pathway (Fig. S1). Moreover, eight significantly upregulated genes were found to be involved in PDT-induced HIF-1 survival signaling [36]. These observations implicate HIF-1α as a key player in the GBCs' resistant response to PDT. We therefore initially proposed that Af would disable the resistance mechanisms controlled or regulated by HIF-1α in the GBCs and thereby potentiate Vp-mediated GBM PDT.

To achieve GBM-targeted co-delivery of Vp and Af, we employed and expanded a technique of 'platelets with photo-controlled release property' which we devised and demonstrated in a previous work [37]. Explained briefly, unengineered platelets are separately loaded with Vp and Af to yield Vp@Plt and Af@Plt, respectively, and the mixture thereof is termed Vp@Plt + Af@Plt. Alternatively, platelets are simultaneously loaded with Vp and Af, which approach is termed (Vp + Af)@Plt. Intravenously injected Vp@Plt + Af@Plt or (Vp + Af)@Plt are distributed to the GBM vasculature via the bloodstream. Laser irradiation (LI) of the GBM generates ROS in the loaded platelets which are immediately activated and form aggregates in the tumor blood vessels, accompanied by rapid and massive offloading of cargo Vp and Af. Note that Af@Plt activation is not induced by LI but is secondary to LI-activated Vp@Plt. Oxidative disruption of the vascular endothelium by ROS facilitates Vp and Af penetration of and spread in the tumor tissue. Once the offloaded drugs are distributed in the tumor cells, a second LI of the GBM causes photodynamic damage of the tumor cells, which is enhanced by Af.

We first used in vitro and in vivo GBM models to demonstrate the strategy of photo-controlled, targeted co-delivery of Vp and Af via platelets for enhanced GBM PDT. Next in the mechanistic study, we set out to prove our original hypothesis that Af might potentiate the photo-cytotoxicity of Vp + LI(690 nm), i.e. Vp-mediated photodynamic action (PDA) through inhibiting the induced HIF-1α. However, our investigation ended up revealing a much more complex picture than had been initially assumed, which involved both Af and Vp blocking a PDA-induced interaction of HIF-1α and the yes-associated protein 1 (YAP). YAP is an important

transcription co-regulator that promotes the expression of genes involved in cell survival and apoptosis suppression and can be specifically inhibited by Vp [25]. An in-depth discussion is made on the novelty and significance of our findings.

## Results

### Photo-controlled co-delivery of Vp and Af via platelets achieved potentiated GBM PDT

#### *Characterization of Vp@Plt, Af@Plt, Vp@Plt + Af@Plt, and (Vp + Af)@Plt*

Vp@Plt and Af@Plt were prepared by incubating isolated mouse platelets ($10^6$/mL) separately with Vp (3 μg/mL in PBS) and Af (10 μM in PBS) for 30 min. (Vp + Af)@Plt were prepared by incubating mouse platelets with a mixture of Vp (3 μg/mL) and Af (10 μM) in PBS for 30 min. The uploading of Vp, Af, and Vp + Af were confirmed by confocal microscopy (Fig. 1A, B). Vp@Plt only exhibited Vp-derived fluorescence and Af@Plt only exhibited Af-derived fluorescence while (Vp + Af)@Plt exhibited both Vp- and Af- derived fluorescence at the same time (Fig. 1A, B). The non-toxic loading concentration for Vp (3 μg/mL) and Af (10 μM) were determined using the CCK-8 test to assay the viability of platelets after incubation with Vp or Af across a range of concentrations (Fig. 1C, D). Under these conditions, loading efficiency was 0.48 μg/$10^6$ platelets for Vp and 0.25 μg/$10^6$ platelets for Af. Vp@Plt were quite stable within 8 h of preparation showing no significant sign of activation and spontaneous release as indicated by the expression of surface CD62p and cellular Vp fluorescence (Fig. 1E, F). Upon LI (690 nm, 0.5 W/$cm^2$, 60 s), Vp@Plt exhibited a spike of ROS generation with concurrent platelet activation and rapid loss of Vp (Fig. 1G-I). Notably, the GBC-conditioned culture medium (GCM) could also induce Vp@Plt activation and discharge of Vp, albeit to a much lesser extent (Fig. 1H, I). On the other hand, Af@Plt also maintained stability within 8 h of preparation without activation and spontaneous release (Fig. 1J, K). Neither LI (690 nm) nor mixing with Vp@Plt had any remarkable effect on Af@Plt (Fig. 1L, M). However, LI (690 nm) on the mixture of Vp@Plt + Af@Plt effected marked platelet activation and rapid loss of Af from the Af@Plt (Fig. 1L, M). Similarly, (Vp + Af)@Plt remained stable showing little sign of platelet activation and spontaneous offloading within 8 h of preparation but exhibited a marked loss of Vp and Af upon LI (690 nm) (Fig. 1N-P).

#### *Photo-triggered, GBM-targeted delivery mediated by Vp@Plt, Vp@Plt + Af@Plt, and (Vp + Af)@Plt*

We next demonstrated photo-controlled drug delivery from Vp@Plt, Vp@Plt + Af@Plt, and (Vp + Af)@Plt to in vitro mouse GBCs (GL261) per an experimental protocol shown in Fig. 2A. Working concentration was 0.48 μg/mL for Vp and 0.25 μg/mL for Af. The GBCs only displayed a low content of Vp, Af, Vp + Af, and Vp + Af following 1 h of treatment of Vp@Plt, Af@Plt, Vp@Plt + Af@Plt, and (Vp + Af)@Plt, respectively (Fig. 2B, C), likely due to a low level of platelet activation and drug release elicited by the GBCs (Fig. 1H, I). In contrast, LI (690 nm, 0.5 W/$cm^2$, 60 s) at the outset of the treatment resulted in sharply increased drug contents in all groups of GBCs but those treated with Af@Plt (Fig. 2B, C), indicating the occurrence of LI-triggered delivery of Vp and co-delivery of Vp & Af to the GBCs from the loaded platelets. The lack of LI-triggered drug delivery by Af@Plt alone (Fig. 2C) is reasonable as LI (690 nm) does not excite Af. Next, the GBCs that had been treated with Vp@Plt exhibited pronounced ROS generation upon a second LI 1 h after the first LI (Fig. 2D), which led to significant cytotoxicity manifested as cell viability loss (WST-8), DNA damage (γH2AX), ER stress (CHOP, GRP78), and apoptosis (Annexin V, Bax & Bcl-2) (Fig. 2E-J). Significantly, photo-controlled co-delivery of Vp and Af by way of Vp@Plt + Af@Plt (Fig. 2E-G) and (Vp + Af)@Plt (Fig. 2H-J) both led to markedly enhanced photo-cytotoxicity over Vp@Plt.

The in vitro results were then validated in mice bearing intra-cranial grafted GBMs per protocols shown in Fig. S4. The animals, according to their assignments, were each given an intravenous bolus injection of Vp@Plt, Af@Plt, (Vp + Af)@Plt, or Vp@Plt + Af@Plt, in 200 μL of PBS. The dosage was 24 μg/kg for Vp and 12.5 μg/kg for Af. After a drug-to-light interval of 1 h, two extra-cranial LI (690 nm, 0.5 W/$cm^2$, 60 s) were applied to each animal at the tumor site at a 2-hr interval. The first LI was meant to induce GBM-targeted, photo-controlled drug delivery and the second LI was for activation of the Vp distributed in the tumor and thereby elicitation of photodynamic damage of the tumor. As shown in Fig. 3A, all animals but those injected with Af@Plt exhibited remarkable drug distribution in the GBMs 2 hrs after the first LI. Notably, the mice injected with Vp@Plt only displayed Vp fluorescence in the GBMs while the mice injected with either (Vp + Af)@Plt or Vp@Plt + Af@Plt displayed both Vp and Af fluorescence in the GBMs, indicating successful co-delivery of the two agents. The lack of Af distribution in the GBMs in the Af@Plt-injected mice is in keeping with the in vitro observation shown in Fig. 2C, which are both ascribed to the fact that Af is not excited by LI (690 nm). Further along, increased drug fluorescence indicating accumulation of delivered drug was observed in all animals but those injected with Af@Plt 24 h after the second LI (Fig. 3B). In agreement with the drug delivery profiles, the mice that had received (Vp + Af)@Plt or Vp@Plt + Af@Plt exhibited more massive and severe tissue necrosis in the GBMs than those that received Vp@Plt 24 h after the second LI, indicating that the

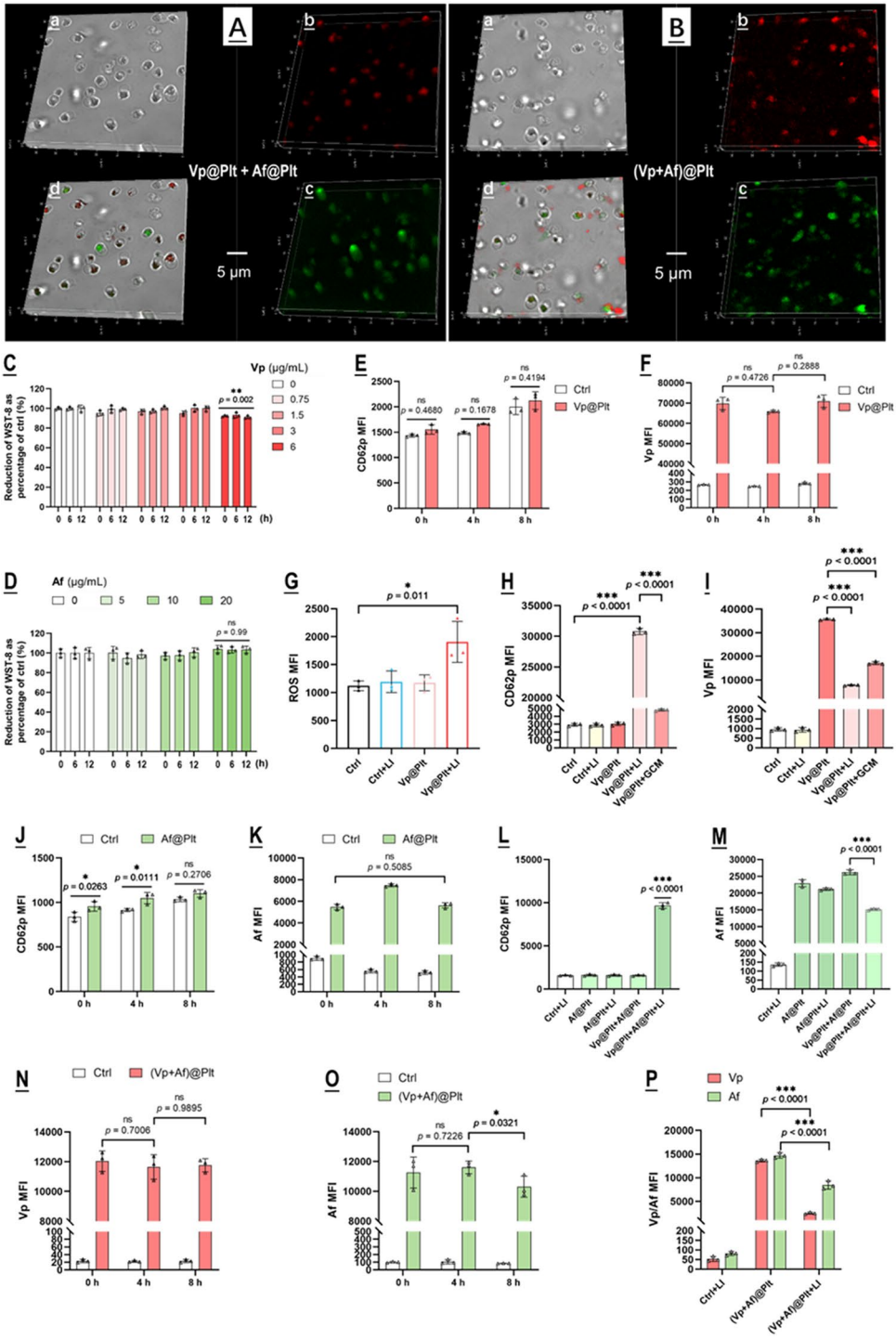


**Fig. 1** Characterization of Vp@Plt, Af@Plt, Vp@Plt + Af@Plt, and (Vp + Af)@Plt. **A** & **B**: Confocal microscopy of Vp@Plt + Af@Plt, and (Vp + Af)@Plt. Vp fluorescence (red) was observed in the Cy5 channel with 650 nm excitation and emission at 670 nm. Af fluorescence (green) was observed in the FITC channel with 488 nm excitation and emission at 520 nm. **a**: Bright field. **b**: Vp-derived fluorescence. **c**: Af-derived fluorescence. **d**: Merge of a, b, and c. **C&D**: Platelets incubated with Vp and Af at a range of concentrations were maintained in PBS and aliquots of the loaded platelets were taken at different time points for viability assay. **E** Spontaneous activation of Vp@Plt over time, indicated by surface CD62P expression. **F**: Spontaneous offloading from Vp@Plt over time, indicated by intracellular Vp content. **G**: ROS generation in the Vp@Plt upon LI (690 nm). **H**: Activation of Vp@Plt by LI (690 nm) and GBC-conditioned culture medium (GCM). **I**: Offloading from Vp@Plt triggered by LI (690 nm) and GCM. **J**: Spontaneous activation of Af@Plt over time, indicated by surface CD62P expression. **K**: Spontaneous offloading from Af@Plt over time, indicated by intracellular Af content. **L**: Activation of Vp@Plt + Af@Plt by LI (690 nm). **M**: LI (690 nm) triggered offloading of Af@Plt in mixture with Vp@Plt but not Af@Plt solo. **N&O**: Spontaneous offloading from (Vp + Af)@Plt over time, indicated by intracellular Vp and Af content. **P**: LI (690 nm) triggered offloading of (Vp + Af)@Plt. Values are means ± standard deviation (SD) ($n = 3$, $^{*}p < 0.05$, $^{**}p < 0.01$, $^{***}p < 0.001$). Representative flow cytometry contour plots for E-P are presented in Fig. S2

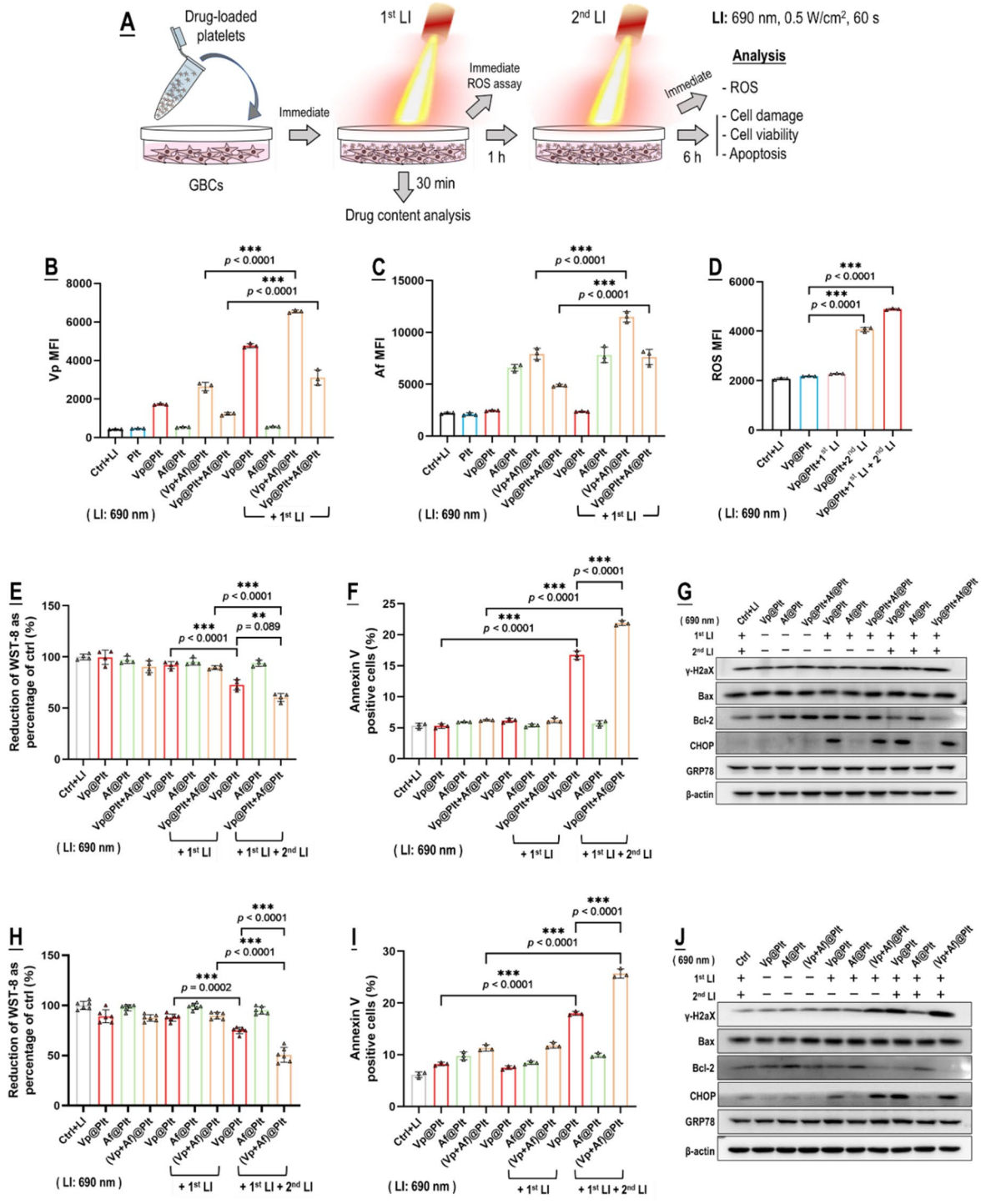


**Fig. 2** Photo-triggered drug delivery from Vp@Plt, Vp@Plt + Af@Plt, and (Vp + Af)@Plt to in vitro GBCs and subsequent photocytoxicity. **A**: Experimental protocol. Briefly, Vp@Plt, Af@Plt, Vp@Plt + Af@Plt, and (Vp + Af)@Plt were separately mixed with GL261 cells and the mixture received two LI (690 nm, 0.5 W/cm$^2$, 60 s) at an interval of 1 h. The GL261 cells were taken out for analysis at indicated time points. **B&C**: Vp and Af contents in the GL261 cells after the first LI, assayed by flow cytometry. **D**: ROS generation in the GL261 cells upon the 1st and 2nd LI. **E**-**G**: Photo-cytotoxicity of Vp@Plt + Af@Plt vs. Vp@Plt and Af@Plt indicated by WST-8 test, annexin v staining, and expression of γH2AX, Bax, Bcl-2, CHOP, and GRP78. **H**-**J**: Photo-cytotoxicity of (Vp + Af)@Plt vs. Vp@Plt and Af@Plt indicated by WST-8 test, annexin v staining, and expression of γH2AX, Bax, Bcl-2, CHOP, and GRP78. Values are means ± standard deviation (SD) ($n = 3$, $^*p < 0.05$, $^{**}p < 0.01$, $^{***}p < 0.001$). Representative flow cytometry contour plots for E-P are presented in Fig. S3. Quantitative analysis of Western blot data in G & J is shown in Fig. S12 & Fig. S13 in the supplement information

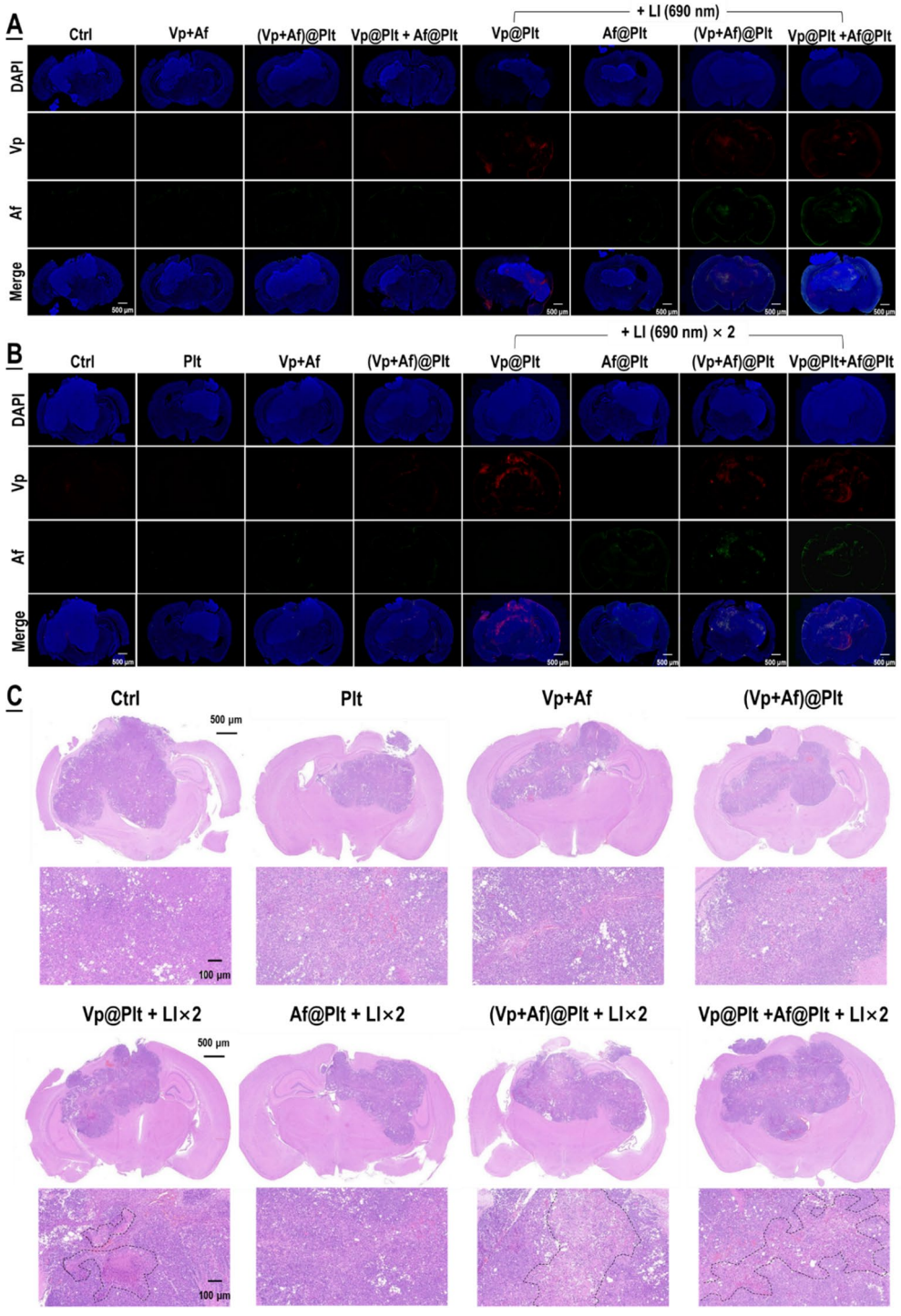


**Fig. 3** Photo-triggered, GBM-targeted drug delivery by Vp@Plt, Vp@Plt + Af@Plt, and (Vp + Af)@Plt and subsequent phototoxicity to the GBM. Experimental protocol is shown in Fig. S3. Briefly, intracranial GBM-bearing mice were intravenously injected with Vp@Plt, Af@Plt, Vp@Plt + Af@Plt, or (Vp + Af)@Plt and, 1 h later, received 2 LI (690 nm, 0.5 W/cm$^2$, 60 s) at the tumor site at a 2-hr interval. Part of the animals were sacrificed 2 hr after the 1st LI and the rest sacrificed 24 h after the 2nd LI. The brains were taken for fluorescent staining, H&E staining and microscopy. **A**: Vp and Af fluorescence in the GBMs 2 hr after the 1st LI. **B**: Vp and Af fluorescence in the GBMs 24 h after the 2nd LI. **C**: H&E staining of the brain and GBM tissues harvested 2 hr after the 1st LI and 24 h after the 2nd LI. Areas circled in the dotted lines are tissues with severe necrosis. Representative higher magnification confocal fluorescent microscopic images of are presented in Fig. S5 & S6

co-delivered Af enhanced Vp-mediated photo-damage of the GBMs (Fig. 3C). By contrast, none of the control animals that had received an intravenous injection of Vp + Af, or (Vp + Af)@Plt, or Vp@Plt + Af@Plt but without LI displayed significant drug distribution, accumulation (Fig. 3A, B), and massive tissue necrosis (Fig. 3C) in the GBMs. Nor did the mice that had received the Af@Plt injection plus LI present massive tissue necrosis in the GBMs they were carrying (Fig. 3C).

#### *Vp@Plt + Af@Plt and (Vp + Af)@Plt achieved more potent GBM-targeted PDT than Vp@Plt*

For evaluation of therapeutic efficacy, mice bearing intracranial grafted GBMs were treated per a protocol illustrated in Fig. 4A. Briefly, the GBM-bearing mice which were divided into six groups, according to their assignments, were each given an intravenous bolus injection of ②Plt, ②(Vp + Af)@Plt, ③Af@Plt, ④Vp@Plt, ⑤(Vp + Af)@Plt, or ⑥Vp@Plt + Af@Plt, in 200 μL of PBS. The dosage was 24 μg/kg for Vp and 12.5 μg/kg b.w. for Af. After a drug-to-light interval of 1 h, the animals in groups ②, ③, ④, ⑤, and ⑥ each received 2 LI (690 nm, 0.5 W/cm$^2$, 60 s) at the tumor site at a 2-hr interval. Two further LI were performed, one 24 h and the other 48 h after the second LI. The animals in group ② only received the first LI 1 h after drug injection. The first LI was meant for GBM-targeted, photo-triggered drug delivery and all the other LI were for activation of the Vp distributed in the tumor and thereby elicitation of photodynamic damage of the tumor. The treatment protocol was performed twice at an interval of 5 days. As shown in Fig. 4B-F, Vp@Plt- mediated PDT (Vp@Plt + LI×4, group ④) showed remarkable anti-GBM efficacy with such manifestations as markedly slowed tumor growth, significant extension of host survival, and much alleviated body weight loss. More importantly, both (Vp + Af)@Plt (group ⑤) and Vp@Plt + Af@Plt (group ⑥) achieved tangibly higher therapeutic efficacy than Vp@Plt (group ④). Particularly, 3 out of the 5 animals in group ⑤ that received (Vp + Af)@Plt + LI×4 and 2 out of the 5 animals in group ⑥ that received Vp@Plt + Af@Plt + LI×4 were still alive at the end of the experiment by which time all otherwise treated animals had already been lost. In contrast, neither (Vp + Af)@Plt + 1st LI (group ②) nor Af@Plt + LI×4 (group ④) exhibited appreciable therapeutic efficacy. Furthermore, gross examination of resected brains showed smaller tumor growths and significantly better preserved brain morphology in groups ④, ⑤ and ⑥ (Fig. 5A). H&E staining also revealed massive tissue necrosis in the tumor grafts in groups ④, ⑤ and ⑥, and there was no apparent brain tissue damage (Fig. 5B). Remarkably, tumor grafts in groups ②, ④, ⑤ and ⑥, at the time of host sacrifice which was 25 days after the last time of drug administration, still displayed appreciable drug retention as indicated by the drug-derived fluorescence (Fig. 5C). These observations are compelling proof that (1) photo-controlled delivery of Vp via Vp@Plt achieved efficacious anti-GBM PDT, (2) photo-controlled co-delivery of Vp and Af, either through (Vp + Af)@Plt or Vp@Plt + Af@Plt achieved more potent anti-GBM PDT than Vp@Plt.

### Both Af and Vp could potentiate GBM PDT through blocking PDT-induced interaction of HIF-1α and YAP in GBCs

#### *Both Af and Vp potentiated photodynamic toxicity in GBCs*

We next set out to demonstrate our original mechanistic hypothesis that Af might potentiate the photo-cytotoxicity of Vp-mediated PDA through blocking the induced HIF-1α. Vp, however, has pharmacological activities (e.g. inhibition of YAP) [38, 39] that would likely bear on its photo-cytotoxicity and the activity of Af. Considering this possibility, we adopted another photosensitizer, chlorin e6 (Ce6) plus 808 nm of excitation light (Ce6 + LI(808)) in parallel with Vp + LI(690 nm) in the mechanistic study. We had previously demonstrated that Ce6 can be excited by LI(808 nm) which does not excite Vp [37]. Herein, as shown in Fig. 6A, Ce6 generated ROS in the GBCs under LI(808 nm) but Vp did not. Af as expected potentiated Ce6's photo-toxicity to the GBCs under LI(808 nm), as was indicated by a marked increase in DNA damage (γH2X & comet assay) and apoptosis (surface annexin v) (Fig. 6B-D). Surprisingly, Vp also potentiated the photo-cytotoxicity of Ce6 under LI(808 nm) (Fig. 6B-D). TEM provided further evidence that both Af and Vp enhanced GBC apoptosis induced by Ce6 + LI(808 nm) (Fig. 6E). These findings suggest that (1) Vp has non-photosensitizing effects that might potentiate the photo-toxicity of itself and other photosensitizers; and (2) the potentiative action of Af might not be limited to Vp-mediated PDA but also apply to other photosensitizers.

#### *PDA induced HIF-1α, which both could be suppressed by Af and Vp*

As mentioned above, our initial hypothesis was that Af might potentiate the photo-cytotoxicity of Vp + LI(690 nm) through repressing the induced HIF-1α. Thus, to begin with, we examined the effect of Af on the gene transcription (mRNA level), protein content, degradation activity (indicated by the levels of PHD2 and P-VHL) of HIF-1α, and its downstream targets in in vitro GBCs following exposure to Vp + LI (690 nm). $CoCl_2$, a widely used hypoxia-mimicking agent that increases HIF-1α by inhibiting the PHD [40], was used for control. As shown in Fig. 7A, HIF-1α mRNA level showed little change following exposure to Vp + LI(690 nm). Paradoxically, there was an obvious increase of HIF-1α protein and its downstream targets (VEGFA, GLUT1, & CA9) (Fig. 7B-E). This apparent inconsistency could only

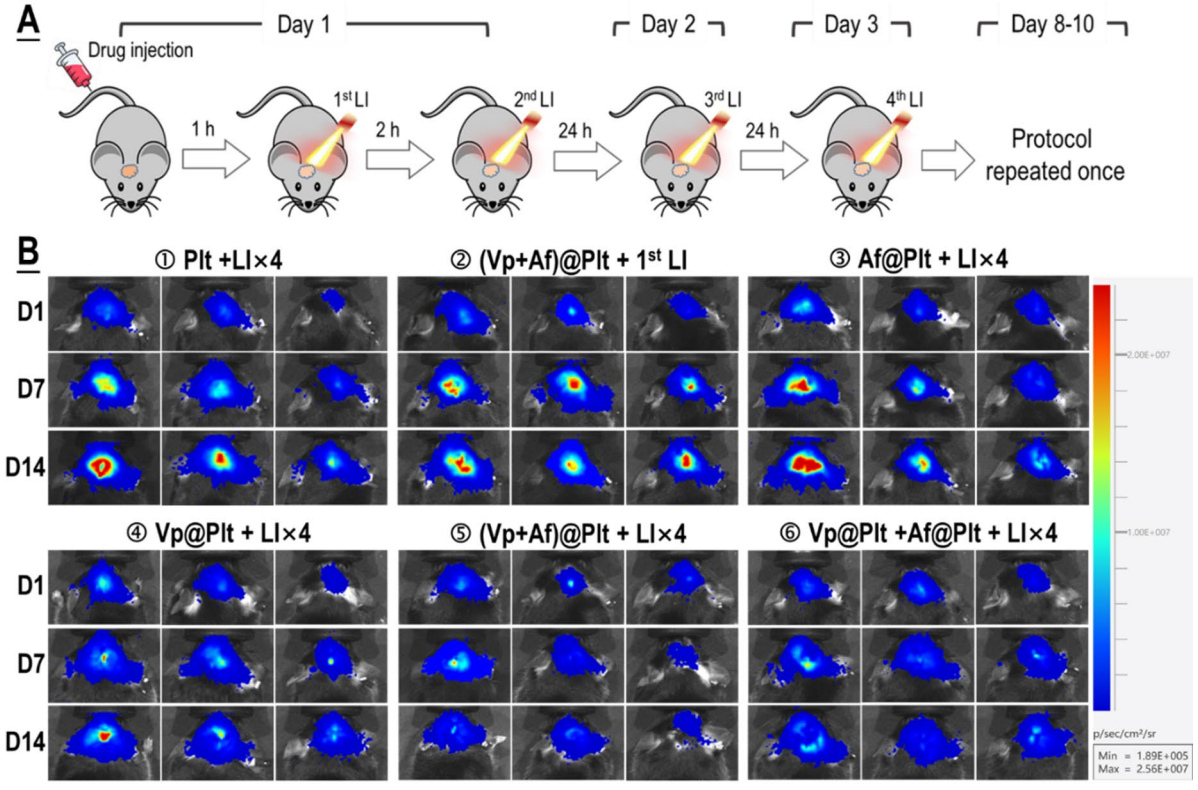


**D**

| Groups | Median survival | |
|---|---|---|
| ① Plt + LI×4 | 27 | $p = 0.0375$ |
| ② (Vp+Af)@Plt + 1st LI | 24 | $p = 0.0038$ |
| ③ Af@Plt + LI×4 | 28 | $p = 0.0382$ |
| ④ Vp@Plt + LI×4 | 38 | |
| ⑤ (Vp+Af)@Plt + LI×4 | undefined | undefined |
| ⑥ Vp@Plt + Af@Plt + LI×4 | 47 | undefined |

**F**

| Groups | Body weight growth rate | |
|---|---|---|
| ① Plt + LI×4 | -2.24% ± 0.24% | $p < 0.0001$ |
| ② (Vp+Af)@Plt + 1st LI | -2.15% ± 0.34% | $p < 0.0001$ |
| ③ Af@Plt + LI×4 | -1.83% ± 0.21% | $p = 0.0003$ |
| ④ Vp@Plt + LI×4 | -0.70% ± 0.17% | |
| ⑤ (Vp+Af)@Plt + LI×4 | 0.17% ± 0.19% | $p = 0.0005$ |
| ⑥ Vp@Plt + Af@Plt + LI×4 | 0.11% ± 0.24% | $p = 0.0009$ |

**Fig. 4** Anti-GBM efficacy of PDT mediated by photo-activated Vp@Plt, Vp@Plt + Af@Plt, and (Vp + Af)@Plt. **A**: Experimental protocol. Briefly, five groups of GBM-bearing animals were intravenously injected with platelets (Plt), Af@Plt, Vp@Plt, (Vp + Af)@Plt, and Vp@Plt + Af@Plt, respectively (①③④⑤⑥). The animals were then subjected to a succession of 4 LI (0.5 W/cm$^2$, 60 s) at intervals at the tumor site. The treatment protocol took 3 days to complete and was repeated once. As control, another group of animals were injected with (Vp + Af)@Plt and only received the 1st LI (②). **B**: Fluorescent images of brain tumors in vivo taken on day 1, 7, and 14 into therapy. GBM-derived luminescence on day 1 and the increase in GBM-derived luminescence up to day 14 was quantified and showed in Fig. S7. **C** & **D**: Survival analysis of treated animals. **E** & **F**: Body weight of treated animals monitored over the therapy duration. Body weight growth rates were calculated by regression analysis. Values were means ± SD ($n = 5$)

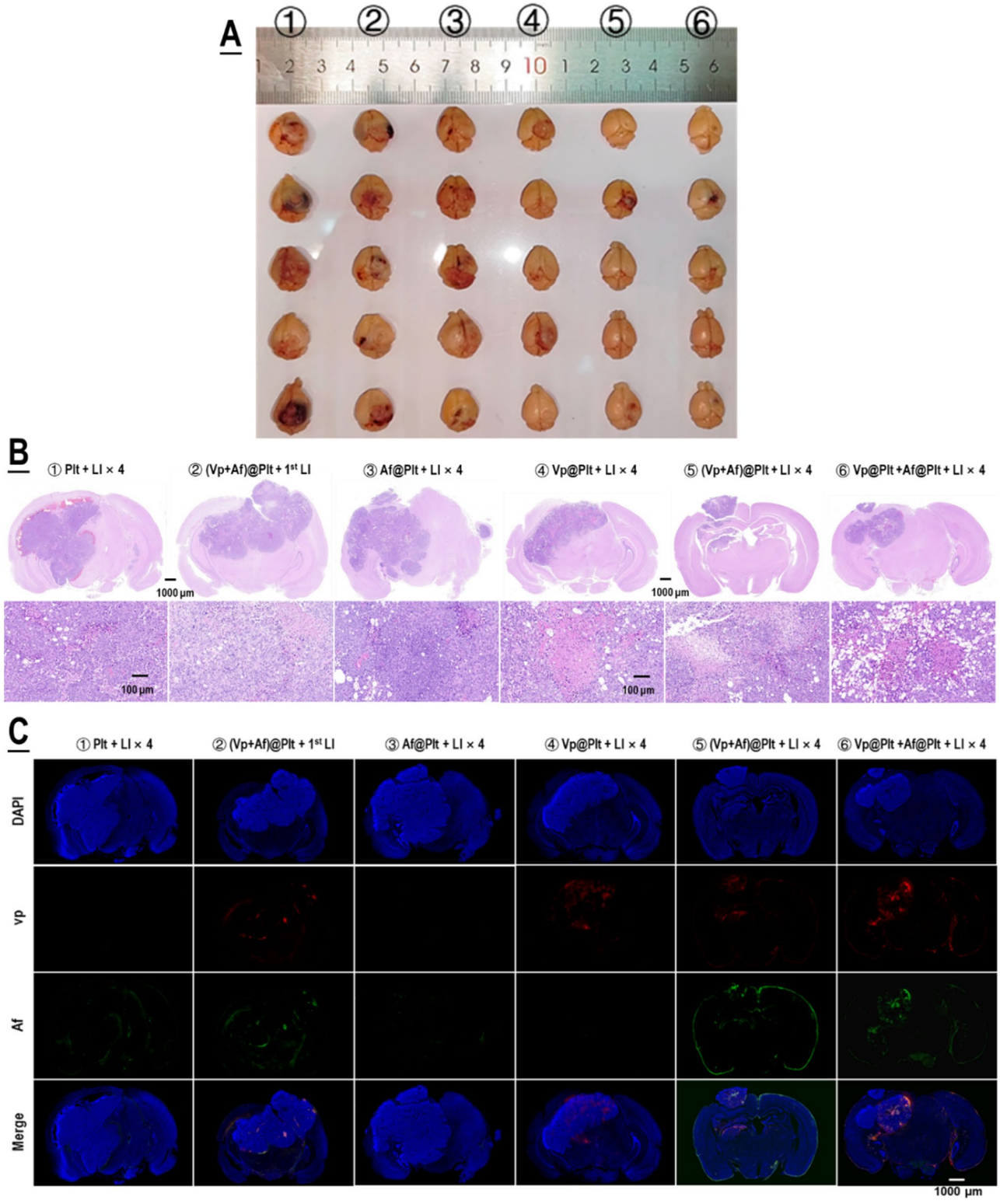


**Fig. 5** Typical morphology of orthotopic GBC graft tumors and tumor drug retention at the end of therapy. **A**: Gross examination of resected brains. **B**: H&E staining of brain tissue slides. **C**: Confocal fluorescent microscopy of brain tissue slides

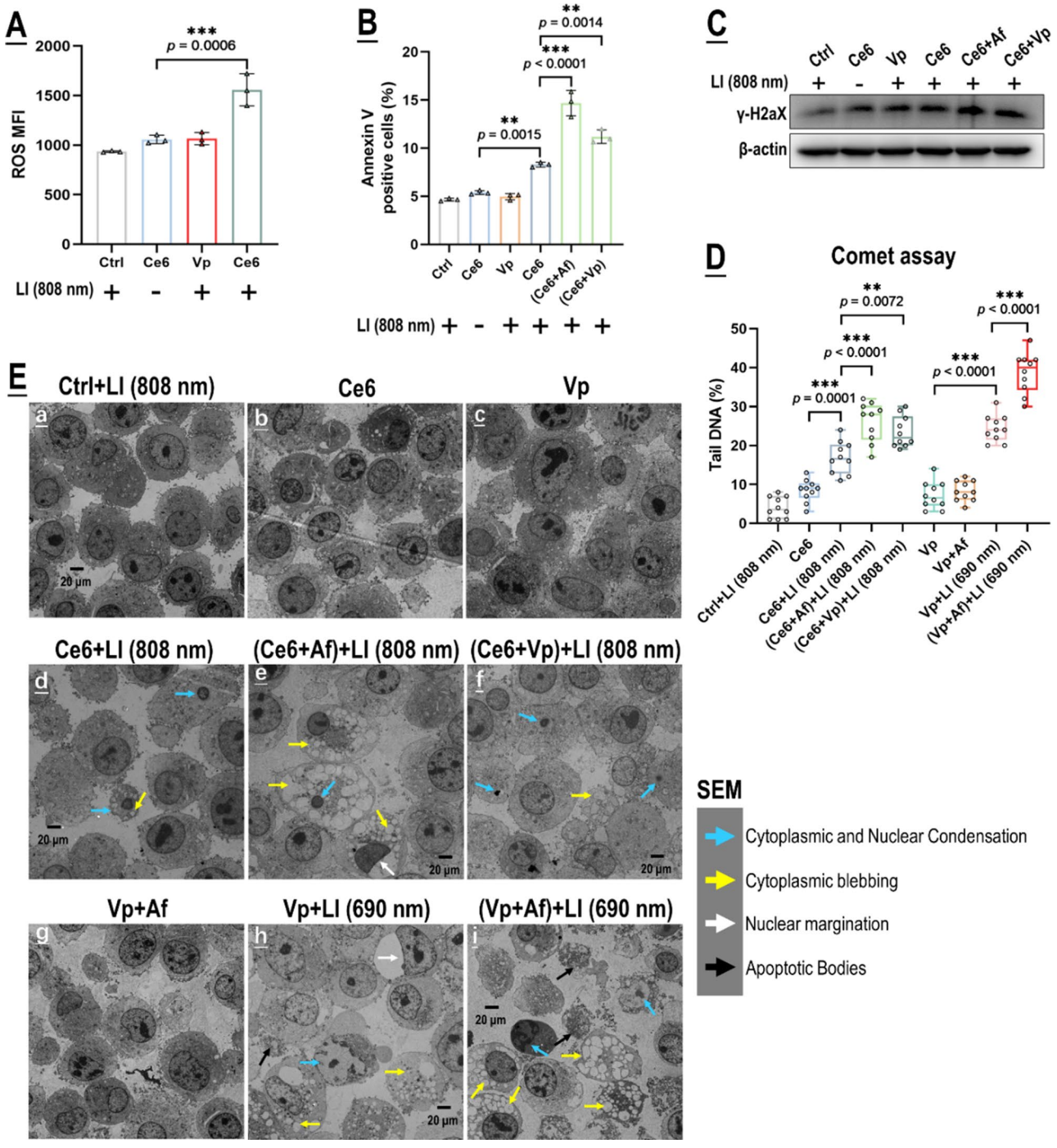


**Fig. 6** Both Af and Vp potentiated the photo-toxicity of Ce6 under LI (808 nm). **A**: Ce6 but not Vp generated ROS under LI (808 nm) in in vitro GL261 cells. Effect of Vp, Ce6, Ce6 + Af, and Ce6 + Vp under LI (808 nm) on cell surface annexin v expression (**B**), γH2AX (**C**), DNA damage indicated by the comet assay (**D**), and cell morphology observed via SEM (**E**). Representative flow cytometry contour plots for **A** & **B** are shown in Fig. S9 A & B. Comet assay images for **D** are shown in Fig. S9C

be attributed to decreased HIF-1α degradation as was indeed indicated by a reduction in PHD2 and P-VHL, the principal enzymes responsible for HIF-1α degradation (Fig. 7F). Af, as expected, alleviated the upregulation of HIF-1α and its downstream targets induced by Vp + LI (690 nm) (Fig. 7E). $CoCl_2$ also upregulated HIF-1α and its downstream targets (Fig. 7E) with consistently decreased PHD2 and P-VHL (Fig. 7F) and these effects were not only alleviated by Af but, interestingly, also by Vp (Fig. 7E, F). This observation suggests that Vp may have non-photosensitizing effects on the PDA-induced HIF-1α and this assumption was substantiated

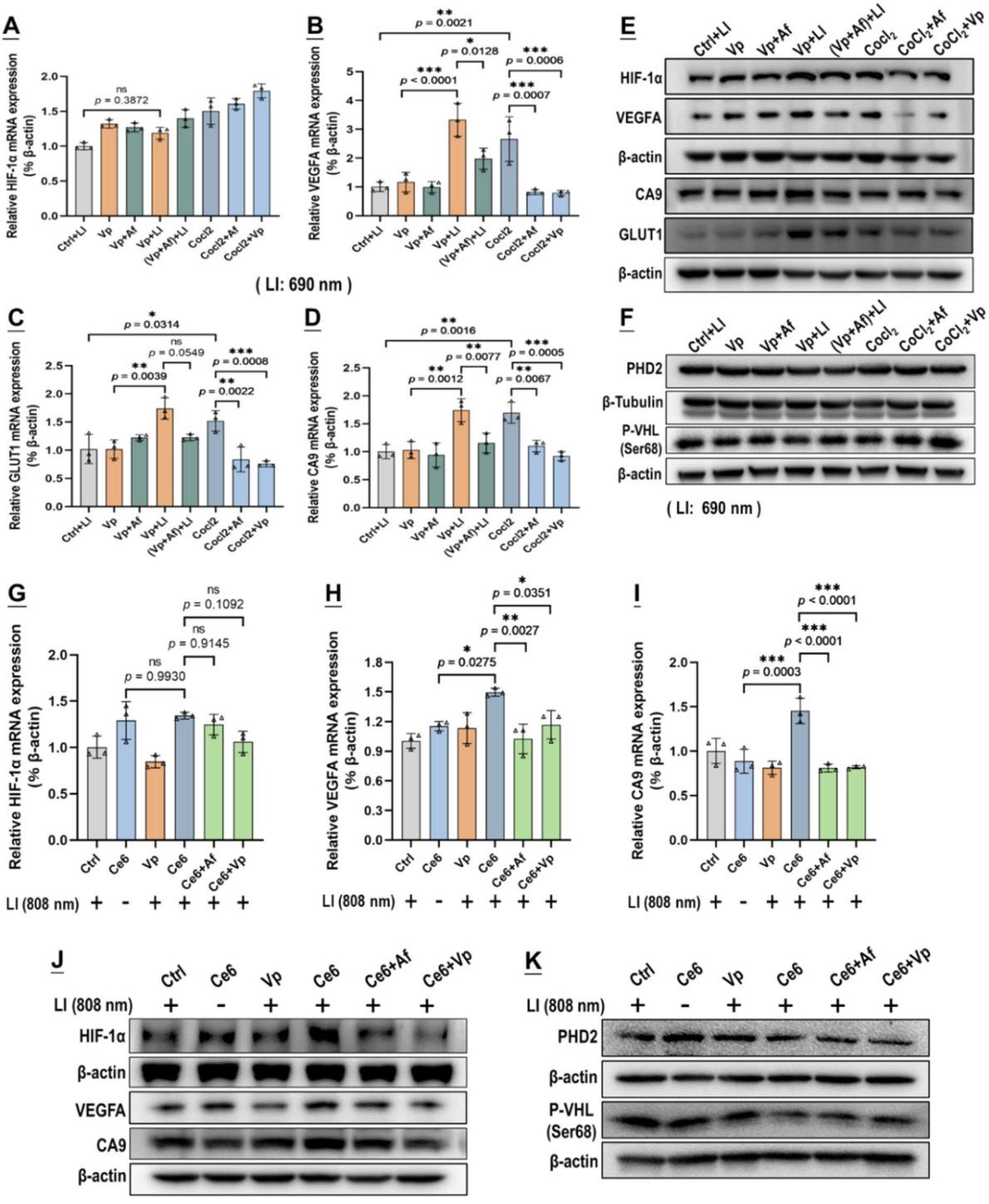


**Fig. 7** Both Vp and Af suppressed HIF-1α induction caused by Vp under LI (690 nm) or Ce6 under LI(808 nm). Effect of Vp and Af on mRNA levels of HIF-1α (**A**), VEGFA (**B**), GLUT1 (**C**), and CA9 (**D**), their protein levels (**E**), and levels of HIF-1α degradation enzymes PHD2 and P-VHL(**F**) in G261 cells exposed to PDA mediated by Vp under LI(690 nm). $CoCl_2$ was used as a control treatment in **A**-**F**. Effect of Vp and Af on mRNA levels of HIF-1α (**G**), VEGFA (**H**), and CA9 (**I**), their protein levels (**J**), and levels of HIF-1α degradation enzymes PHD2 and P-VHL (**K**) in G261 cells exposed to PDA mediated by Ce6 under LI (808 nm). Values were means ± SD ($n = 3$, $^{*}p < 0.05$, $^{**}p < 0.01$, $^{***}p < 0.001$). Quantitative analysis of Western blot data in F is shown in Fig. S14 in the supplement information

by the use of Ce6 + LI(808 nm). As shown in Fig. 7G-K, Ce6 + LI(808 nm), like Vp + LI(690 nm), had little effect on HIF-1α mRNA level but resulted in a remarkable increase in HIF-1α protein and its downstream targets (VEGFA & CA9), as well as decreased PHD2 and P-VHL indicative of diminished HIF-1α degradation. Significantly, both Af and Vp markedly suppressed the upregulation of HIF-1α protein and its downstream targets with little bearing on HIF-1α mRNA (Fig. 7G-J), and this effect was accompanied by an increase in P-VHL indicating recovered HIF-1α degradation (Fig. 7K). The in vitro results were well reflected in the in vivo orthotopic GBMs exposed to Vp@Plt + LI (690 nm), which exhibited enhanced expression of HIF-1α and VEGFA, which was alleviated by Af delivered either in the form of (Vp + Af)@Plt or Vp@Plt + Af@Plt (Fig. 8A). To recap briefly, PDA induced HIF-1α by reducing its degradation rather than upregulating its gene transcription, and this effect could be antagonized by both Af and Vp leading to increased HIF-1α degradation.

#### *PDA induced YAP, which could both be suppressed by Vp and Af*

In light of the above observations and the fact that Af is a recognized HIF-1α inhibitor and Vp is a well-known YAP inhibitor [25, 26], we suspected that PDA might induce an interplay of HIF-1α and YAP in the GBCs. To explore this notion, we surveyed the gene transcription (mRNA level), protein content, and degradation activity of YAP in in vitro GBCs exposed to PDA. Under Vp + LI (690 nm), there was an upsurge in YAP mRNA but, paradoxically, no increase in YAP protein (Fig. 9A & B). This inconsistency could only be explained by increased YAP degradation which was clearly indicated by a marked increase in YAP-Ser127-P and P-LATS1 (Fig. 9B). (Note: P-LATS1 is the activated formed of LATS1, which triggers YAP phosphorylation at Ser127 (YAP-Ser127-P), resulting in cytoplasmic retention and degradation [41]). Vp, an agent known to promote YAP degradation [38, 39], was strongly indicated to be the actor underlying the decreased YAP protein by another two lines of evidence. First, Vp alleviated $CoCl_2$-induced YAP protein level without affecting YAP mRNA (Fig. 9A & B). Second, Ce6 + LI(808 nm) also induced YAP and its downstream targets (Survivin & CTGF) as well and Vp alleviated the induced protein level of YAP and its downstream targets without affecting YAP mRNA (Fig. 9C-G). Significantly, Af also repressed the induced YAP protein level and its downstream targets without affecting YAP mRNA (Fig. 9C-G), and both Vp and Af resulted in heightened YAP degradation as was indicated by a marked increase in YAP-Ser127-P and P-LATS1 (Fig. 9D). The orthotopic GBMs displayed enhanced YAP and CTGF expression following exposure of Vp@Plt + LI (690 nm) (Fig. 8B), which appeared to be inconsistent with the observed YAP decrease in in vitro GBCs (Fig. 9B). This inconsistency, as is discussed later, is attributed to the aggravated hypoxia in the tumor tissue as a result of PDT. Notwithstanding, the enhanced YAP and CTGF expression was alleviated by Af delivered either in the form of (Vp + Af)@Plt or Vp@Plt + Af@Plt (Fig. 8B), which is in keeping with the in vitro findings. To recap briefly, PDA induced YAP via upregulating its gene expression, which effect could be antagonized both by Vp and Af leading to increased YAP degradation.

A synthesis of the findings in subsections 2.2 and 2.3 suggest that PDA might induce an interplay of HIF-1α and YAP, which begins with heightened YAP gene transcription and leads to reduced degradation of both factors; both Af and Vp could block this interaction therefore increasing the degradation of HIF-1α and YAP. There has been study suggesting that HIF-1α can physically interact with YAP in cancer and non-cancer cells under hypoxic stress, promoting the functions of both factors [34, 42, 43]. We wondered PDA might induce a similar interaction in GBCs and found relevant evidence which is presented below.

#### *PDA elicited an interplay of HIF-1α and YAP which could both be blocked by Af and Vp*

The GBCs exhibited a conspicuous nuclear co-localization of HIF-1α and YAP following exposure of Vp + LI (690 nm), or Ce6 + LI (808 nm), or $CoCL_2$ (Fig. 10A). Co-IP assay also identified increased binding of HIF-1α and YAP both under Vp + LI (690 nm) and Ce6 + LI (808 nm), which could be both suppressed by Vp and Af (Fig. 10B, C). Notably, the Co-IP assay also demonstrated the changes in HIF-1α and YAP protein levels at the same time following exposure to PDA (Fig. 10B, C). Both Vp + LI (690 nm) and Ce6 + LI (808 nm) triggered an increase of HIF-1α which could be alleviated by AF. But YAP behaved differently. Under Vp + LI (690 nm), the YAP level declined, which was ascribed to Vp-mediated degradation and compounded by the addition of Af (Fig. 10B). Under Ce6 + LI (808 nm), the YAP level increased, which could be both suppressed by Af and Vp (Fig. 10C). Overall, these observations are consistent with those shown in Figs. 7 and 9. Silencing of HIF-1α and YAP by siRNA produced a further line of evidence of an HIF-1α-YAP interplay induced by PDA. Knock-down of HIF-1α and YAP both alleviated the nuclear co-localization of HIF-1α and YAP elicited by Ce6 + LI (808 nm) (Fig. 11A) and suppressed the induction of HIF-1α, YAP, and their downstream targets (Fig. 11B). Also, WST-8 assay (Fig. 11C) and cell surface annexin v assay (Fig. 11D) indicated that knock-down of HIF-1α and YAP both potentiated the photo-cytotoxicity of Ce6 + LI (808 nm) much like Af and Vp did (Fig. 6).

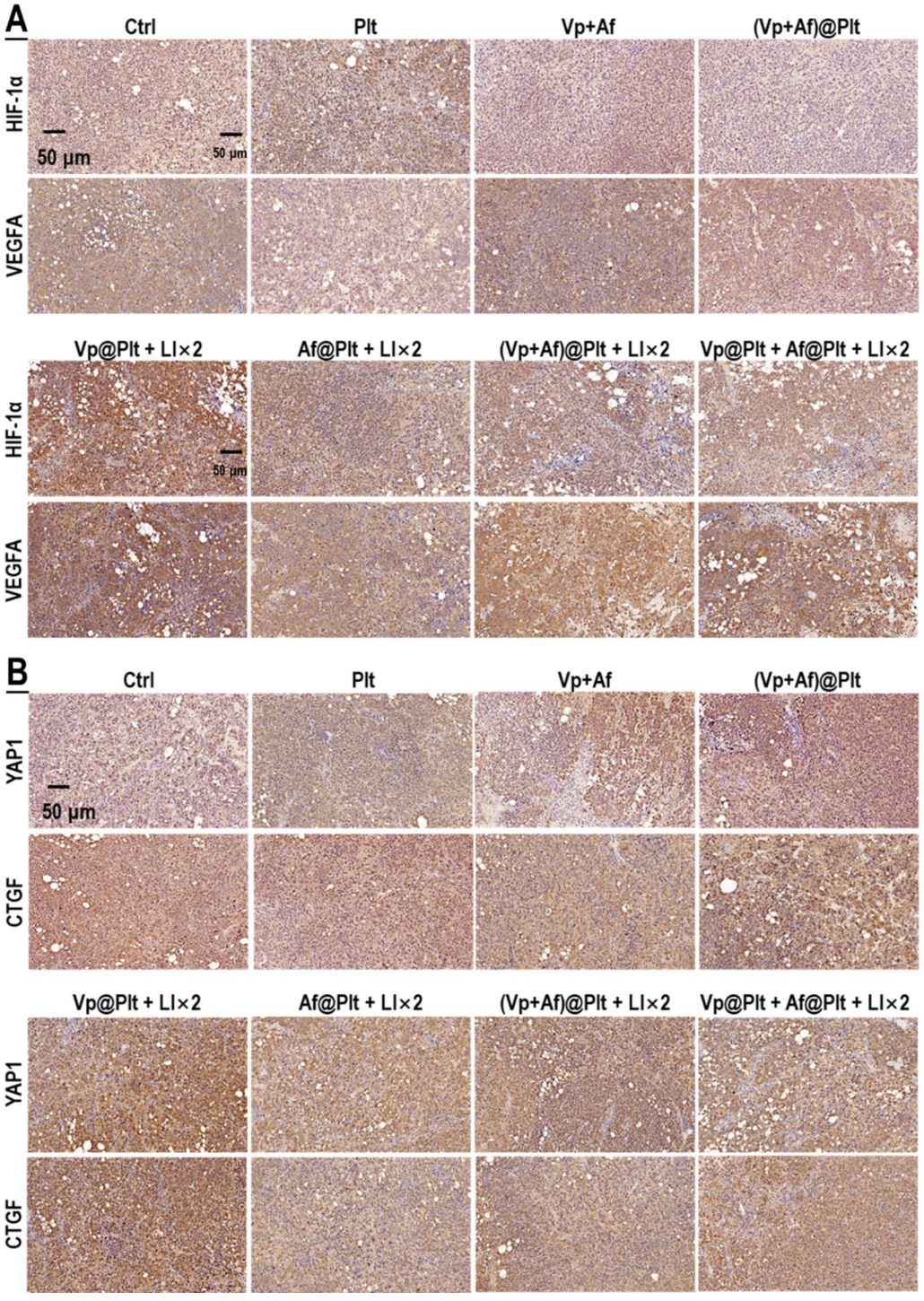


**Fig. 8** Af delivered in the form of (Vp + Af)@Plt and Af@Plt + Vp@Plt both suppressed the induction of HIF-1α and YAP caused by Vp@Plt under LI (690 nm) in intracranial GBM tissues. Experimental protocol is shown in Fig. S4. Briefly, intracranial GBM-bearing mice were intravenously injected with Vp@Plt, Af@Plt, Vp@Plt + Af@Plt, or (Vp + Af)@Plt and, 1 h later, received 2 LI (690 nm, 0.5 W/cm$^2$, 60 s) at the tumor site at a 2-hr interval. The animals were sacrificed 24 h after the 2nd LI. The brains were taken for immunohistochemical (IHC) staining of HIF-1α, VEGFA (**A**), YAP, and CTGF (**B**)

To recap, PDA elicited an interaction of HIF-1α and YAP which boosted their nuclear distribution and thereby increased the expression of their downstream targets. Af or Vp could block this interaction impacting both HIF-1α and YAP and potentiate the PDA-induced toxicity in the GBCs. In light thereof, we posited that the HIF-1α-YAP interaction might be part of the cellular response to PDA-inflicted cell damage, which is

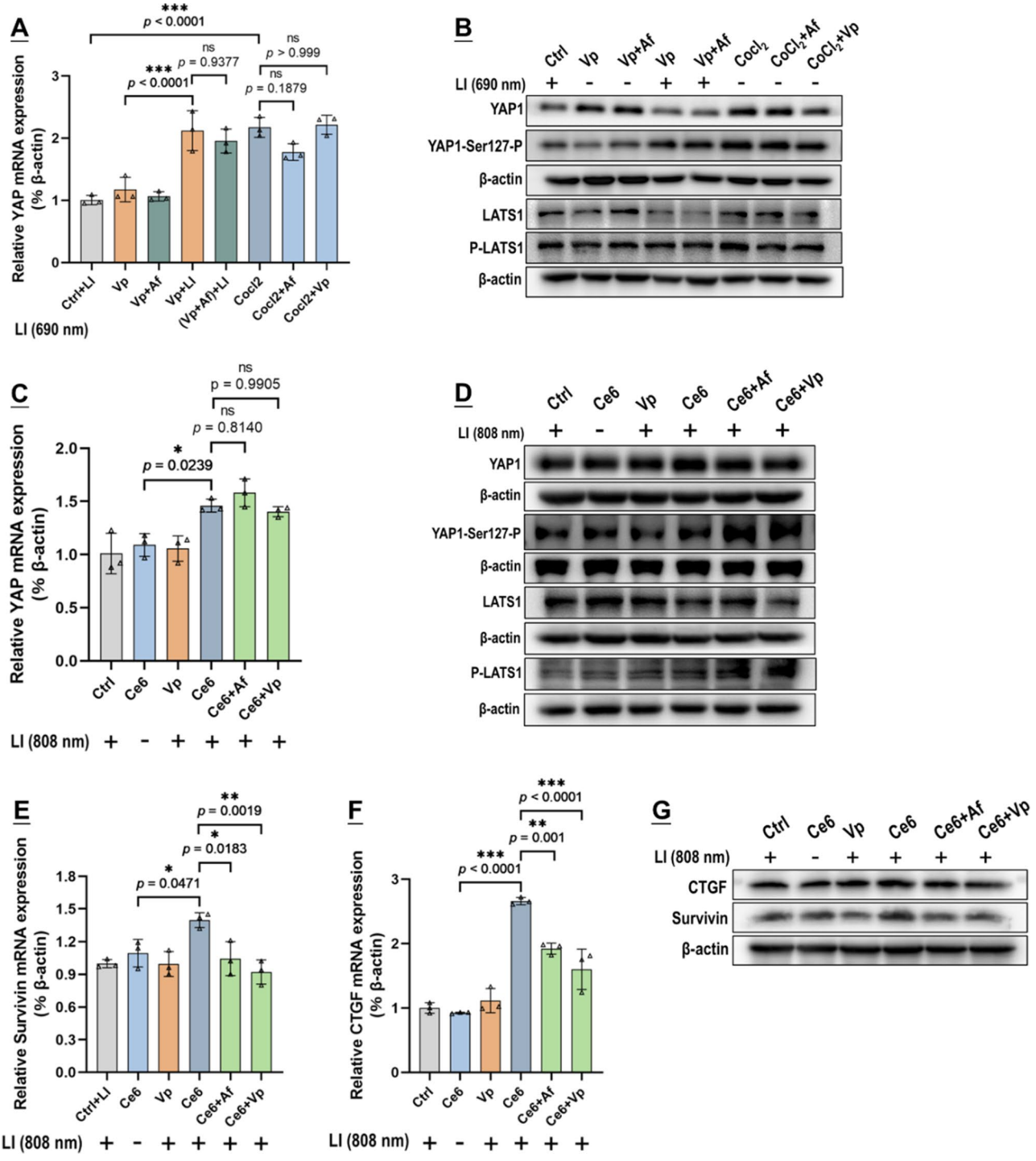


**Fig. 9** Both Vp and Af suppressed YAP induction caused by Vp under LI (690 nm) or Ce6 under LI(808 nm). Effect of Vp and Af on YAP mRNA level (**A**), protein levels of YAP, YAP-Ser127-P, LATS1, and P-LATS1 (**B**) in G261 cells exposed to PDA mediated by Vp under LI (690 nm). $CoCl_2$ was used as a control treatment in **A** & **B**. Effect of Vp and Af on YAP mRNA level (**C**), protein levels of YAP, YAP-Ser127-P, LATS1, and P-LATS1 (**D**), mRNA levels of Survivin (**E**) and CTGF (**F**), and their protein levels (**G**) in G261 cells exposed to PDA mediated by Ce6 under LI(808 nm). ($n = 3$, $^{*}p < 0.05$, $^{**}p < 0.01$, $^{***}p < 0.001$). Quantitative analysis of Western blot data in B & D is shown in Fig. S15 in the supplement information

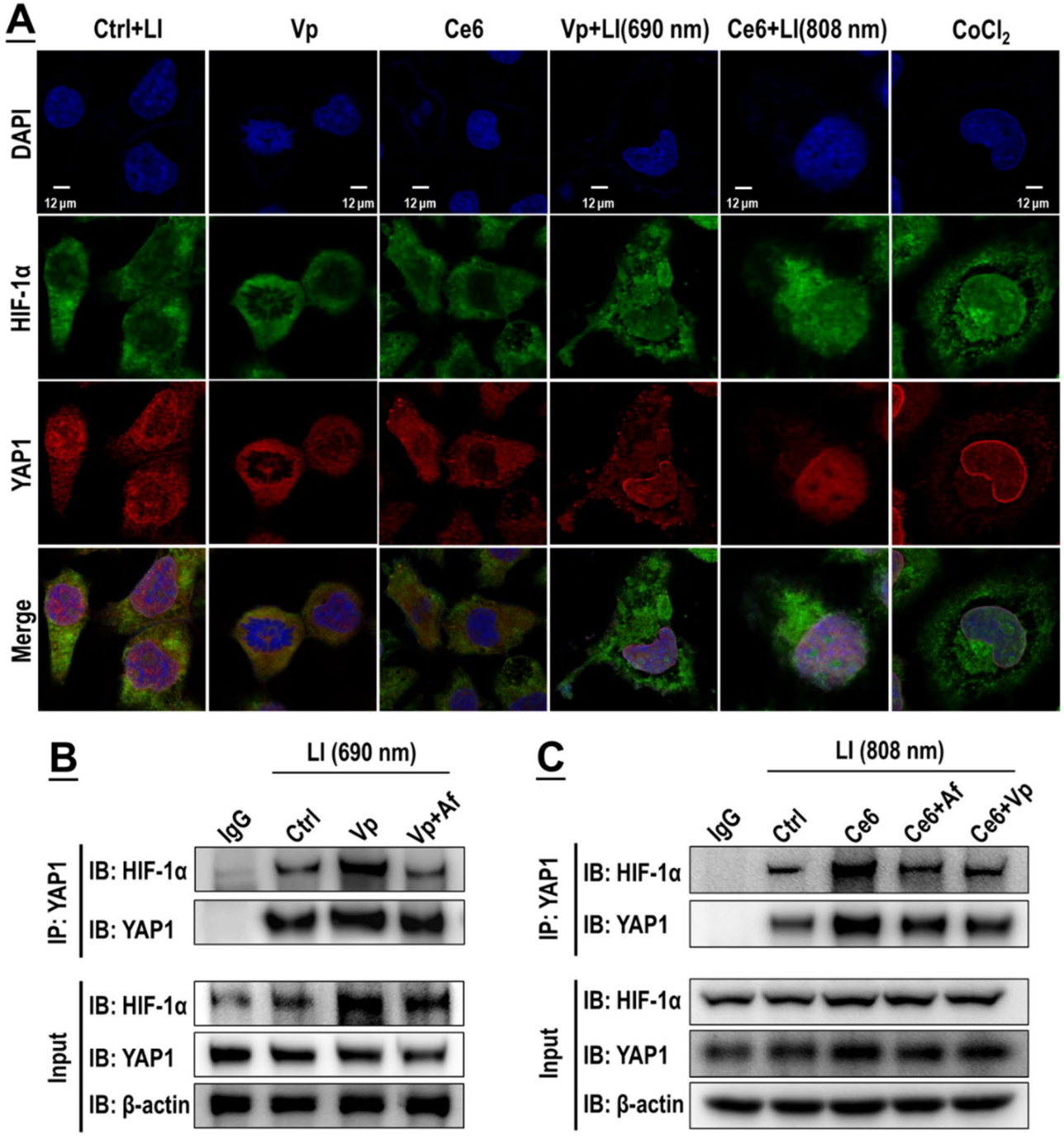


**Fig. 10** Vp under LI (690 nm) and Ce6 under LI (808 nm) both stimulated an interplay of HIF-1α and YAP, which could be blocked by Vp or Af. **A**: Enhanced fluorescent co-localization of HIF-1α and YAP in the nucleus. $CoCl_2$ was used as a control treatment. **B&C**: Co-immunoprecipitation (CO-IP) analysis indicated increased binding of HIF-1α and YAP, which effect could be both suppressed by Vp and Af

mobilized for damage repair and sustaining cell survival. Evidence is as follows.

#### *PDA-elicited HIF-1α-YAP interaction resulted from DNA damage and led to upregulated DNA repair activity*

As pronounced DNA damage was identified following exposure to PDA (Fig. 2), we blocked the DNA damage response in PDA-exposed GBCs employing pharmacologic inhibitors of the ATR, ATM, and DNA-PK, which are major DNA damage sensors [44, 45]. As shown in Fig. 12A-C, inhibition of each of the 3 sensors could suppress the upregulation of HIF-1α and YAP and their downstream targets either induced by Vp + LI (690 nm) or Ce6 + LI (808 nm). On the other hand, SMUG1 and

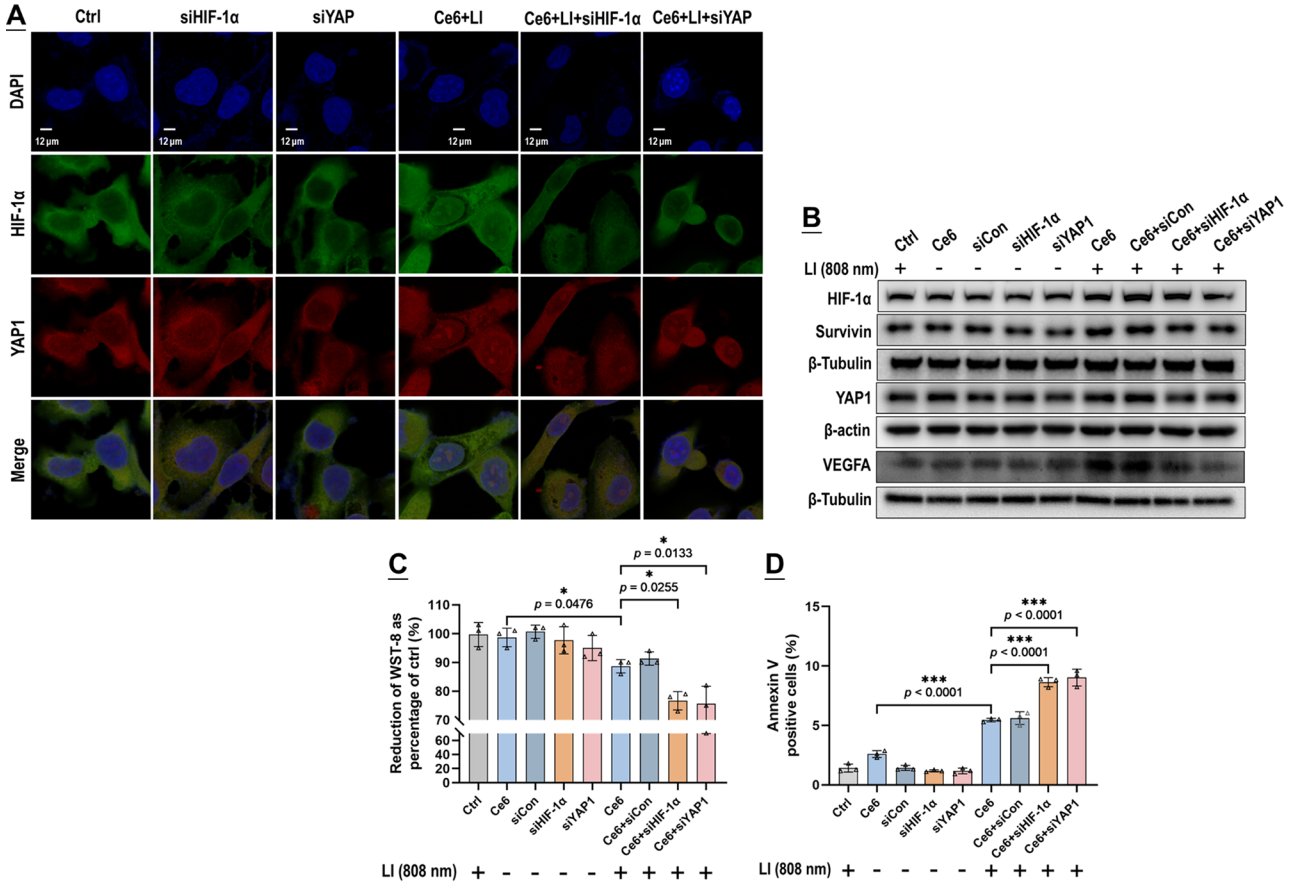


**Fig. 11** Knock-down of HIF-1α and YAP both prevented the interplay of HIF-1α and YAP stimulated by Ce6 under LI (808 nm) and potentiated the photo-cytotoxicity. Knock-down of HIF-1α and YAP both alleviated fluorescent co-localization of HIF-1α and YAP in the nucleus (**A**), decreased the expression of HIF-1α, VEGFA, YAP, and Survivin (**B**), and led to enhanced photo-cytotoxicity indicated by WST-8 assay (**C**) and surface annexin v staining (**D**). Values were means ± SD ($n = 3$, $^{*}p < 0.05$, $^{***}p < 0.001$). Representative flow cytometry contour plots for **D** are shown in Fig. S10

DNA ligase IV (LIG4) are key enzymes involved in nuclear DNA repair [46, 47]. Both Af and Vp markedly suppressed the induction of the two enzymes either caused by Vp + LI (690 nm), or Ce6 + LI (808 nm), or $CoCl_2$ (Fig. 12D-E). Consistently, knock-down of HIF-1α and YAP both suppressed the induction of SMUG1 and LIG4 caused by Ce6 + LI (808 nm) (Fig. 12F). In short, the HIF-1α-YAP interaction was elicited for mobilization of DNA repair which could be both blunted by Af and Vp.

## Discussion

In the first part of this work, we realized highly efficient GBM-targeted co-delivery of Af and Vp through a strategy of 'platelets with photo-controlled release property' and demonstrated that the co-delivered Af significantly enhanced Vp-mediated, GBM-targeted PDT in lab mice (Fig. 13). This strategy, originally devised in one of our previous work [37], relies on stable loading of the cargo drugs in the platelets and exploits the PDA-generated ROS to trigger platelet activation and cargo offloading, thereby achieving photo-controlled, GBM-directed drug delivery. The delivery of small-molecule drugs and the co-delivery approaches are the two major advancements from the original strategy. Platelets contain three main types of granules that can serve as depots for internalized drugs, i.e. the alpha granules, approximately 60–80 per platelet, dense granules, 4–6 per platelet, and lysosomes [48, 49]. The small-molecule drugs employed herein were Af and Vp, both of which could be stably loaded in platelets in quantity. Af interacts with platelet granules primarily by localizing to dense granules, where it acts as a serotonin analog [50, 51]. Af is a derivative of acridine with lysosomotropism which means this agent due to its weak basic nature can also accumulate in lysosomes [52]. On the other hand, Vp upon uptake by platelets is believed to target the alpha granules and dense granules which are released upon platelet activation [53, 54]. During platelet activation, Af- and/or Vp-laden granules undergo exocytosis, releasing their contents into the extracellular space. It is the properties of Af and Vp to target specific granules that enable their stable carriage by platelets. It is a reasonable generalization that

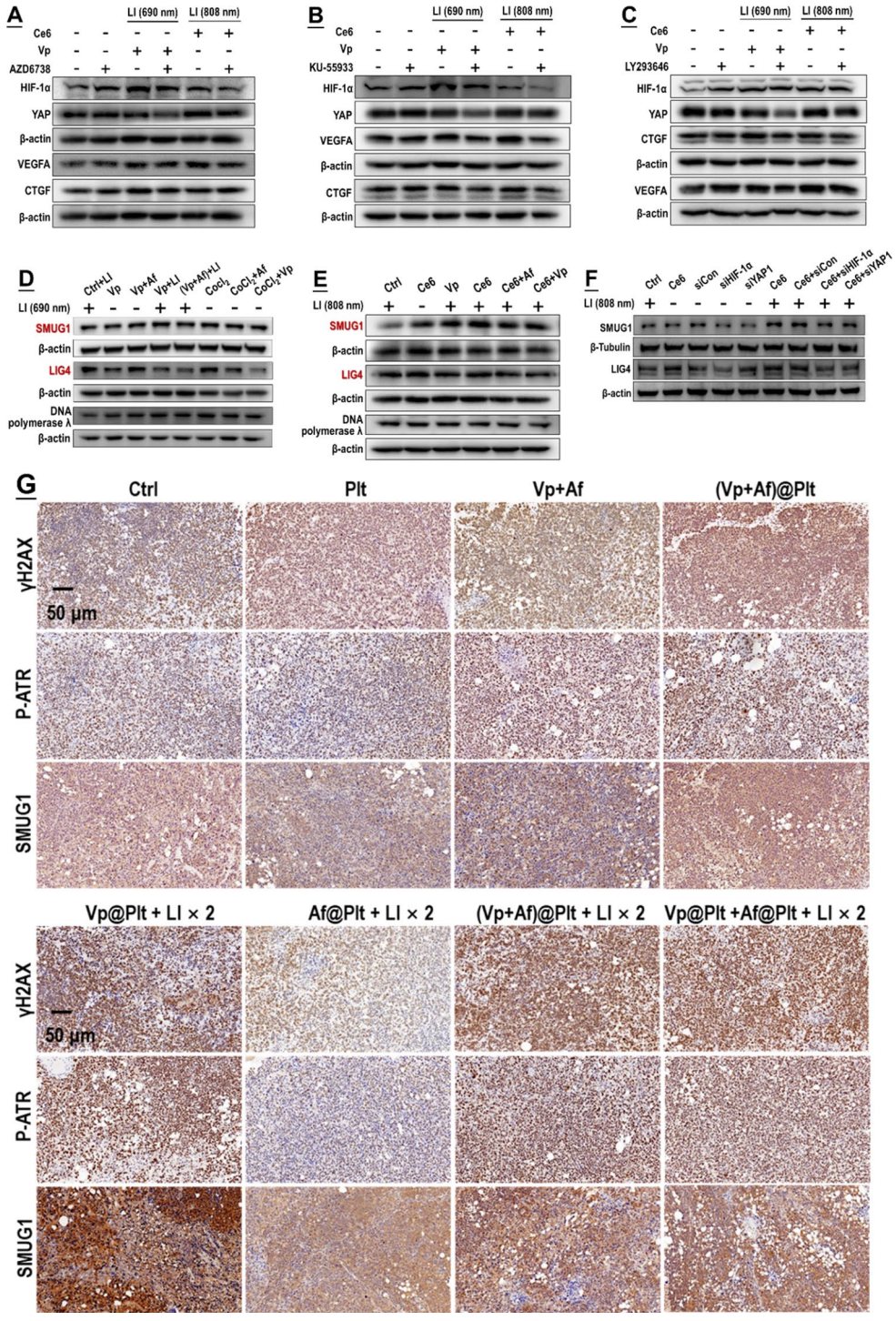


**Fig. 12** Induction of HIF-1α and YAP by PDA was a downstream event to DNA damage and led to upregulation of DNA damage repair activity. **A**-**C**: Pharmacological blocking of DNA damage sensors (i.e. ATR, ATM, and DNA-PK) alleviated induction of HIF-1α and YAP both caused by Vp under LI (690 nm) and Ce6 under LI(808 nm). AZD6738, KU-55,933, and LY293646 are inhibitors of the ATR kinase, ATM kinase, and DNA-PK, respectively. **D&E**: Both Af and Vp blocked induction of DNA repair enzymes (i.e. SMUG1 and LIG4) caused by Vp under LI(690 nm) or Ce6 under LI(808 nm). **F**: Knock-down of HIF-1α and YAP both prevented the induction of SMUG1 and LIG4 caused by Ce6 under LI(808 nm). **G**: Af delivered in the form of (Vp + Af)@Plt and Af@Plt + Vp@Plt both suppressed the induction of SMUG1 and LIG4 caused by Vp@Plt under LI(690 nm) and potentiated the DNA damage (indicated by γH2AX and P-ATR expression) in intracranial GBM tissues. Experimental protocol is shown in Fig. S4. Briefly, intracranial GBM-bearing mice were intravenously injected with Vp@Plt, Af@Plt, Vp@Plt + Af@Plt, or (Vp + Af)@Plt and, 2 h later, received 2 LI (690 nm, 0.5 W/cm$^2$, 60 s) at the tumor site at a 2-hr interval. The animals were sacrificed 24 h after the 2nd LI. The brains were taken for IHC staining of γH2AX, P-ATR, SMUG1, and LIG4

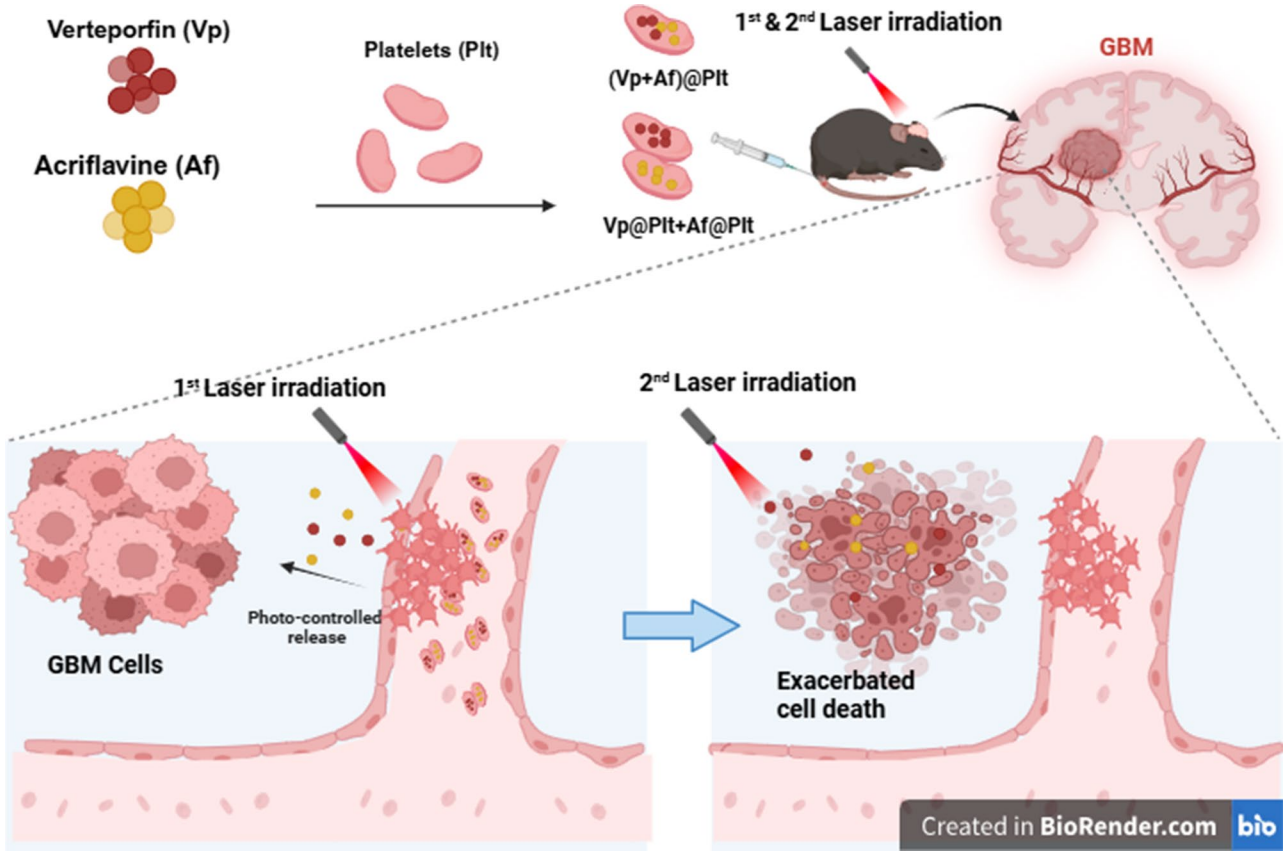


**Fig. 13** Schematic illustration of potentiation of anti-GBM PDT by double blocking of HIF-1α-YAP interplay through co-delivery of Af and Vp via platelets with photo-controlled release property

any other drugs that target the platelet granules can potentially be carried by platelets for active delivery as long as they do not cause platelet activation and toxicity per se. Co-delivery of Af and Vp was achieved via two approaches i.e. (Vp + Af)@Plt and Vp@Plt + Af@Plt. While both approaches proved to be efficacious in terms of GBM-targeted delivery and PDT, Vp@Plt + Af@Plt would be more flexible in potential translation as this approach allows more freedom in dosage adjustment and choice of drug combination. Both approaches also showed no signs of systemic adverse effects (Fig. S8). Initially, our rationale for co-delivering Af with Vp was to use Af to potentiate Vp-mediated photodynamic toxicity to the GBCs by simply inhibiting the induced HIF-1α. As it turned out, however, the Vp-mediated PDA did not just induce HIF-1α but an interplay of HIF-1α and YAP of which Vp is a potent inhibitor. Thus, Vp served dual purposes both to wreak photodynamic cell damage and block the induced HIF-1α-YAP interplay together with Af.

HIF-1α is believed to be regulated primarily through oxygen availability. Under normoxic conditions, prolyl hydroxylases (PHDs) hydroxylate HIF-1α, leading to its degradation via the VHL ubiquitin-proteasome pathway. In contrast, hypoxia inhibits this hydroxylation, allowing HIF-1α to accumulate, dimerize with HIF-1β, and activate target genes involved in metabolism, angiogenesis, and cell survival [55–57]. HIF-1α also interacts with various cofactors and transcription factors that further modulate its activity and gene expression in response to the tumor microenvironment [57, 58]. YAP is regulated primarily through the Hippo signaling pathway and mechanotransduction. YAP1 levels are directly controlled by the canonical Hippo kinases, MST1/2 and LATS1/2, which modulate its cytoplasmic retention and proteasomal degradation [59, 60]. YAP functions as a transcriptional co-activator, primarily binding to the TEAD proteins to promote the expression of oncogenic genes involved in cell proliferation, survival, and metastasis [61, 62]. HIF-1α has been reported to interact with YAP primarily under hypoxic stress but details are lacking about the mechanism involved. YAP by itself can hardly enter the nucleus as it lacks the canonical nuclear localization signals (NLS) [63]. HIF-1α was found to act as a direct carrier to promote YAP's translocation into the nucleus, allowing YAP to protect cells from DNA damage during hypoxia in canine kidney cells [33]. YAP was also suggested to stabilize HIF-1α and enhance its transcriptional

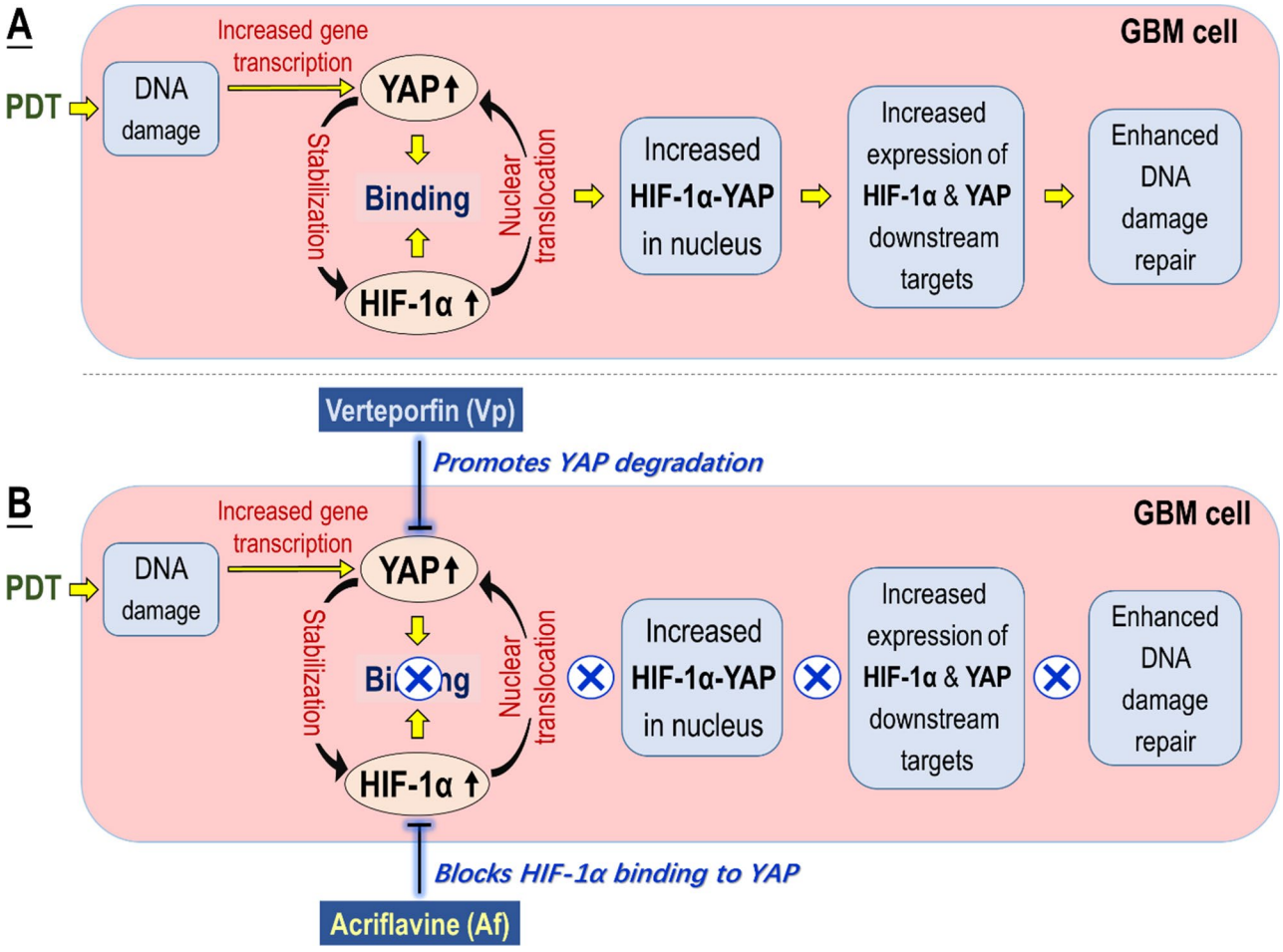


**Fig. 14** Schematic illustration of the HIF-1α-YAP interaction, its upstream cause and downstream outcome (**A**), and the effects of Vp and Af thereon (**B**)

activity, contributing to cellular responses to hypoxia, such as protecting against DNA damage and apoptosis in canine kidney cells and papillary thyroid cancer cells [33, 42]. Af can bind to HIF-1α, preventing its dimerization with HIF-1β and inhibiting its transcriptional activity [26]. Vp inhibits YAP primarily by increasing the levels of 14-3-3σ, a chaperone protein that sequesters YAP in the cytoplasm, preventing its nuclear translocation and subsequent interaction with other factors such as TEAD [38, 39, 64]. Vp may also directly alter YAP conformation, further disrupting its ability to bind to other proteins [64].

In light of the above knowledge, the latter, mechanistic part of our work demonstrated that a mutually promotional interaction of HIF-1α and YAP was induced by PDA both mediated by Vp + LI(690 nm) and Ce6 + LI(808 nm) under normoxic conditions as a result of DNA damage and this interaction led to escalated DNA damage repair activities regulated by HIF-1α and YAP (Fig. 14). This interplay started with an upsurge in YAP level due to increased gene expression, which case differs significantly from those under hypoxic stress where it is initiated by HIF-1α accumulation due to depressed degradation [33, 43, 65]. The induced YAP bound to HIF-1α and the binding appeared to help both YAP and HIF-1α. On one hand, binding to YAP might stabilize HIF-1α by protecting it from degradation by PHD and PVHL which are constantly active under normoxic condition. On the other hand, binding to HIF-1α might assist in the nuclear translocation of YAP which lacks the canonical NLS. Thus, the outcome of the binding of HIF-1α and YAP was increased nuclear presence of both factors leading to enhanced gene expression of their downstream targets, among which were key enzymes involved in DNA damage repair e.g. SMUG1 and LIG4. SMUG1 is a glycosylase that removes uracil from single- and double-stranded DNA in nuclear chromatin, thus contributing to base excision repair while LIG4 is a key enzyme required for DNA double-strand break repair [46, 47]. Our work further revealed that Af might block HIF-1α from binding to YAP leaving HIF-1α to rapid degradation under normoxic condition and the unbound YAP is sequestered in the cytoplasm undergoing degradation. Vp, on the other hand, might directly and potently promote the degradation of YAP thus

leaving the HIF-1α unprotected from rapid degradation under nomoxia. Hence, Af and Vp might synergize with each other to block the PDA-induced HIF-1α-YAP interplay in the GBCs and thereby severely reduce nuclear translocation of both factors, resulting in depletion of the DNA repair enzymes, and ultimately exacerbating PDT-induced DNA damage and cell death. It should be pointed out that YAP is constitutively expressed in GBM cells and it is generally a hypoxic tissue environment inside the in vivo GBMs with a basal activity of HIF-1α, which is unlike the normoxic in vitro condition. It is reasonable to assume that there is a basal activation of the HIF-1α-YAP interaction in the in vivo GBM cells to promote survival in the hypoxic local environment. PDT would aggravate hypoxia in the GBM tissue due to oxygen consumption and destruction of tumor blood vessels by the platelet aggregates, leading to enhanced HIF-1α-YAP interaction in the GBCs. This might explain why the orthotopic GBMs still displayed enhanced YAP and CTGF expression following exposure of Vp@Plt + LI (690 nm) (Fig. 8B), which was inconsistent with the in vitro results shown in Fig. 9B. The mechanistic study also featured the innovative approach of adopting Ce6 + LI (808 nm) in parallel with Vp + LI (690 nm). Ce6 + LI (808 nm) induced the same cellular responses as Vp + LI (690 nm) only minus Vp's non-photosensitizing effects on YAP. It was through comparing the cellular responses of Vp + LI (690 nm) and Ce6 + LI (808 nm) + Vp that we were able to identify Vp's effect on the interplay of HIF-1α and YAP. Regarding the mechanism of PDA mediated by Ce6 under 808 nm excitation, it is well documented that Ce6 can be excited upon two-photo absorption though Ce6 shows no absorption at 808 nm [66–68]. Ce6 is also a potent sonosensitizer and we have incorporated Ce6 in nanoparticles to achieve targeted sonodynamic therapy (SDT) of GBM [69, 70]. But interestingly, Ce6-mediated SDT did not induce the HIF-1α-YAP interaction in the GBCs as observed following Ce6-mediated PDT [70]. Finally, the mutually promotional interplay of HIF-1α and YAP was also induced in the human U251 GBM cells following exposure to Ce6 + LI (808 nm), which could be blocked by both Af and Vp (Fig. S11). This proves the relevance of our findings in human GBM. One caveat from our work is that extra-cranial LI was adopted for the ease of operation. Although the extra-cranial LI worked to good effects on GBM models in mice which have a very thin layer of bone in their skulls, it has difficulty penetrating the think and dense human cranial bone, rendering it impractical for clinical use. However, this problem may be overcome by the interstitial PDT [71, 72].

## Conclusions

Af and Vp can be adequately co-delivered in GBM via unengineered platelets in a photo-controlled manner. GBM cells can mobilize a mutually promotional interaction of HIF-1α and YAP to bolster repair of PDT-inflicted DNA damage. Af can synergize with Vp to potentiate GBM PDT through double blocking of the HIF-1α-YAP interaction.

## Materials & methods

Reagents, antibodies, and their respective suppliers are detailed in Supplementary Table 1.

### Cell culture

GL261-luciferase (GL261-luc) cells and U251 cells were purchased from the Cell.

Bank of Shanghai Institutes for Biological Sciences (Shanghai, China). Cells were maintained in the DMEM medium with 10% fetal bovine serum (QmSuero/Tsingmu.

Biotechnology, Wuhan). All cell lines were maintained in a humidified incubator with 5% $CO_2$ at 37 °C and passaged.

### Animals

Male C57BL/6J mice aged 4–6 weeks were purchased from the Laboratory Animal Center of Hubei Province (Hubei, China). Animal handling and experimental procedures were in line with protocols approved by the Animal Care Committee at Wuhan University.

### Preparation and characterization of platelets with Vp@Plt, Af@Plt, and (Vp + Af)@Plt

Mouse platelets (Plt) from whole blood were prepared from male C57BL/6 mice (5–6 weeks of age, 22 ~ 24 g) through gradient centrifugation according to published protocols [37]. Platelets loaded with Vp, Af, or Vp&Af (Vp@Plt, Af@Plt, or (Vp + Af)@Plt) were obtained by incubating platelets ($1 \times 10^6$) with 3 μg/mL of Vp, Af, or a mixture of both in 1 mL of PBS for 30 min at room temperature. Vp@Plt + Af@Plt and (Vp + Af)@Plt were placed in confocal dishes, respectively, left to stand for 30 min to allow the platelets to precipitate, and photographed using a confocal microscope. Vp fluorescence (red) was observed in the Cy5 channel with 650 nm excitation and emission at 670 nm. Af fluorescence (green) was observed in the FITC channel with 488 nm excitation and emission at 520 nm.

For determination of intra-platelet drug content and platelet activation, loaded platelets were maintained in PBS for 4 and 8 h at room temperature before getting assayed by flow cytometry for Vp and Af fluorescence, and immunofluorescent staining of surface CD62P which is a marker of platelet activation.

### Drug delivery by platelets with photo-controlled drug release property in vitro

Vp@Plt, Af@Plt, or (Vp + Af)@Plt ($1 \times 10^6$ of each in 1 mL of PBS in EP tubes) were either irradiated with laser (690 nm 0.5 W/cm$^2$) for 60 s or incubated with GBM cell-conditioned medium (GCM) for 30 min before getting assayed by flow cytometry for ROS generation, Vp and Af fluorescence, and immunofluorescent staining of surface CD62P. To verify the drug release from the loaded platelets to GBM cells, drug-loaded platelets were added to GL261 cells in multi-welled plates at a ratio of 5:1 and the mixture was immediately irradiated with laser light (690 nm, 0.5 W/cm$^2$, 60 s). The mixture was maintained for 30 min before taking out for flow cytometry analysis of drug fluorescence in the GL261 cells. To evaluate platelets with photo-controlled drug release property-mediated photodynamic toxicity to GBM cells, the mixture of drug-loaded platelets and GL261 cells was first laser-irradiated. After 1 h, the culture medium was removed and, after a rinse with PBS, replaced with fresh culture medium. A second time of laser irradiation was then applied to the GL261 cells. The GL261 cells were taken out immediately for determination of intracellular ROS level, or 5 h later, for analysis of DNA damage, cell viability, and cell apoptosis. ROS production was determined by flow cytometry analysis of staining of 2′,7′-dichlorofluorescein diacetate (DCFDA). DNA damage was evaluated by comet assay according to the assay kit manufacturer's instructions and western blotting (WB) analysis of H2A histone family member X (γ-H2AX). Cell viability was assayed by the CCK-8 test according to the assay kit manufacturer's instructions. Cell apoptosis was observed with transmission electron microscopy (TEM) and assayed by annexin-v staining and WB analysis of B-cell lymphoma-2 (Bcl-2) and Bcl-2-associated X (Bax).

### Drug delivery by platelets with photo-controlled drug release property to GBM grafts in mice

Male C57BL/6J mice at four weeks of age (14–18 g) were used for intracranial GBM models. The establishment of intracranial tumors was performed according to published protocols [73]. Once the tumor volume reached approximately 500 mm$^3$, the tumor-bearing mice were randomly assigned to various treatment groups. The animals, according to their designation, received intravenous injections of unloaded platelets, Vp + Af, Vp@Plt, Af@Plt, (Vp + Af)@Plt or Vp@Plt + Af@Plt each in 200 μL of PBS per mouse. The dosage was calculated to be 0.48 μg of Vp or 0.25 μg of Af in $10^6$ platelets per mouse of 20 g of body weight. For studying drug distribution, Animals received laser irradiation (1st LI) at the tumor site 1 h after the injection. At 2 h after the 1st LI, 3 animals out of each group were sacrificed and brains were harvested for fluorescent imaging. The other 3 animals received a second time of laser irradiation (2nd LI) 2 h after the 1st LI. At 24 h after the 2nd LI, all remaining animals were sacrificed and brains were harvested for fluorescent imaging and H&E staining.

### Efficacy of GBM-targeted PDT mediated by Vp@Plt, Vp@Plt + Af@Plt, and (Vp + Af)@Plt

Intracranial GBM grafts of GL261-luc cells were established as described above. On day 14 post-implantation, tumor-bearing animals were randomly assigned to 6 groups (5 mice per group). Animals were intravenously injected with 200 μL per mouse of PBS containing unloaded platelets, Vp@Plt, Af@Plt, (Vp + Af)@Plt, and Vp@Plt + Af@Plt respectively. The dosage was calculated to be 0.48 μg of Vp or 0.25 μg of Af in $10^6$ platelets per mouse of 20 g. The animals were then subjected to a succession of 4 times of extracranial laser irradiation (690 nm, 0.5 W/cm2, 60 s) at the tumor site (Fig. 4A). The first time laser irradiation (1st LI) was performed 1 h after drug administration to induce Vp@Plt and (Vp + Af)@PIt activation and ensuing Vp and Af release in the intracranial GBM. Two hr later when the released Vp and Af was supposed to have achieved adequate distribution in the GBM tissue, laser irradiation was performed another 3 times (1st, 2nd, and 3rd LI) at an interval of 24 h to achieve PDT efficacy. The full protocol took 3 days to complete and was repeated once on days 8–10.

For control, one group of animals injected with (Vp + Af)@Plt only received the first time of laser irradiation for each treatment. The animals were observed daily until they reached a moribund state, at which time they were sacrificed and their brains and vital organs taken for subsequent histopathologic analysis. Body weight was taken every day throughout the experiment period and brain tumor growth was monitored via weekly fluorescent imaging for the initial two weeks. For imaging, mice under nembutal anesthesia were administrated with luciferin (D-Luciferin potassium salt, 150 mg/kg) via intraperitoneal injection, and then imaged 10 min after injection.

### Both Af and Vp blocked PDA-induced HIF-1α-YAP mutual promotion

Either 0.48 μg/mL Vp alone or Vp combined with 0.25 μg/mL Af was added to GL261 cells and incubated for 1 h and then irradiated or not with laser light (690 nm, 0.5 W/cm$^2$, 60 s). Alternatively, either 10 μg/mL chlorin e6 (Ce6) alone or Ce6 combined with Vp or Af was added to GL261 cells and incubated for 1 h and then irradiated or not with laser light (808 nm, 0.5 W/cm$^2$, 60 s). For the positive control, either 200 μM Cocl2 alone or Cocl2 combined with Vp or Af was added to GL261 cells and incubated for 7 h. Confocal microscopy was applied to

observe the co-localization between HIF-1α with YAP, and co-immunoprecipitation (Co-IP) was applied to identify the occurrence of HIF-1α-YAP interaction. The mRNA and protein levels of target genes were analyzed by real-time quantitative polymerase chain reaction (qPCR) and WB, respectively. The primer sequences are listed in Supplementary Table 2.

### HIF-1α-YAP mutual promotion leads to GBM resistance to PDT

Small interfering RNA (siRNA) targeting HIF-1α, YAP, and NC were designed and synthesized by JTSbio (Wuhan, China). Lipofectamine 8000 (Beyotime) was used to transfect the corresponding siRNA into the cells according to the protocol, cells were cultured for 48 h before Vp- or Ce6- mediated PDT. To investigate the effect of DNA damage inhibitor on HIF-1α-YAP mutual promotion, cells were firstly cultured with 10 μM of KU-55,933 (ATM inhibitor), 0.3 μM of AZD6738 (ATR inhibitor) and 10 μM of NU 7026 (DNA-PK inhibitor), respectively, for 2 h before Vp- or Ce6- mediated PDT. The protein levels of HIF-1α, YAP, and DNA repair-related enzymes (DNA ligase IV, and glycosylase) were subsequently detected by WB.

### Statistical analysis

Data analysis and graph plotting were conducted using GraphPad Prism 8. Group comparisons were performed using one-way analysis of variance (ANOVA) and two-way ANOVA. Kaplan–Meier survival curves and the log-rank test were used for survival analysis.

## Supplementary Information

The online version contains supplementary material available at https://doi.org/10.1186/s12951-025-03395-x.

Supplementary Material 1

#### Author contributions

Jie Guo: Investigation; Methodology; Validation; Formal analysis; Draft writing. MengFei Wang: Investigation; Data curation and Visualization; Draft writing. ShenJun Yuan: Investigation; Resources, Draft writing. Ke Li & Quan Zhang: Methodology; Validation; animal care. HuiMei Lei: Data curation; animal care. JiaLin Wu: Software; Data curation. Yonghong Xu: have drafted the work or substantively revised it; Xiao Chen: Conceptualization; study design; Writing – review & editing; Supervision, Funding acquisition.

#### Funding

Support from The National Natural Science Foundation of China (NSFC) (No. 82272718) to XC and the Natural Science Foundation of Hubei Province (No.2023AFB453) to SJY is gratefully acknowledged.

#### Data availability

No datasets were generated or analysed during the current study.

## Declarations

#### Ethics approval and consent to participate

Not applicable.

#### Consent for publication

Not applicable.

#### Competing interests

The authors declare no competing interests.

#### Author details

[1]Department of Pharmacology, School of Basic Medical Sciences, Wuhan University, Donghu Avenue No.185, Wuhan 430072, China
[2]Echo Lab, Department of Ultrasound Imaging, Renmin Hospital of Wuhan University, Wuhan, China
[3]Department of Pathology, The Central Hospital of Wuhan, Tongji Medical College, Huazhong University of Science and Technology, Wuhan 430014, China
[4]Center for Lab Teaching, School of Basic Medical Sciences, Wuhan University, Donghu Avenue No.185, Wuhan 430072, China
[5]Department of Anatomy and Embryology, School of Basic Medical Sciences, Wuhan University, Donghu Avenue No.185, Wuhan 430072, China
[6]Institute of Ophthalmological Research, Department of Ophthalmology, Renmin Hospital of Wuhan University, Wuhan 430060, China
[7]Hubei Provincial Key Laboratory of Developmentally Originated Disease, Wuhan 430072, China

Received: 10 December 2024 / Accepted: 15 April 2025
Published online: 22 May 2025

#### References

1. Thakkar JP, Dolecek TA, Horbinski C, Ostrom QT, Lightner DD, Barnholtz-Sloan JS, et al. Epidemiologic and molecular prognostic review of glioblastoma. Cancer Epidemiol Biomarkers Prev. 2014;23(10):1985–96.
2. Lieberman F. Glioblastoma update: molecular biology, diagnosis, treatment, response assessment, and translational clinical trials. F1000Res. 2017;6:1892.
3. Angom RS, Nakka NMR, Bhattacharya S. Advances in glioblastoma therapy: an update on current approaches. Brain Sci. 2023;13(11):1536.
4. Lan Z, Li X, Zhang X, Glioblastoma. An update in pathology, molecular mechanisms and biomarkers. Int J Mol Sci. 2024;25(5):3040.
5. Gunasegaran B, Ashley CL, Marsh-Wakefield F, Guillemin GJ, Heng B. Viruses in glioblastoma: an update on evidence and clinical trials. BJC Rep. 2024;2(1):33.
6. Petrecca K, Guiot MC, Panet-Raymond V, Souhami L. Failure pattern following complete resection plus radiotherapy and Temozolomide is at the resection margin in patients with glioblastoma. J Neuro-Oncol. 2013;111(1):19–23.
7. Thon N, Tonn JC, Kreth FW. The surgical perspective in precision treatment of diffuse gliomas. OncoTargets Ther. 2019;12:1497–508.
8. Gunaydin G, Gedik ME, Ayan S. Photodynamic Therapy—Current limitations and novel approaches. Front Chem. 2021;9:691697.
9. Correia JA-O, Rodrigues JA-O, Pimenta SA-OX, Dong T, Yang Z. Photodynamic therapy review: principles, photosensitizers, applications, and future directions. Pharmaceutics. 2021;13(9):1332.
10. Yoo JO, Ha KS. New insights into the mechanisms for photodynamic therapy-induced cancer cell death. Int Rev Cell Mol Biol. 2012;295:139–74.
11. Allison RR, Moghissi K. Photodynamic therapy (PDT): PDT mechanisms. Clin Endosc. 2013;46(1):24–9.
12. Castano AP, Mroz P, Hamblin MR. Photodynamic therapy and anti-tumour immunity. Nat Rev Cancer. 2006;6(7):535–45.
13. Kwiatkowski S, Knap B, Przystupski D, Saczko J, Kędzierska E, Knap-Czop K, et al. Photodynamic therapy – mechanisms, photosensitizers and combinations. Biomed Pharmacother. 2018;106:1098–107.
14. Van Straten D, Mashayekhi V, De Bruijn HS, Oliveira S, Robinson DJ. Oncologic photodynamic therapy: basic principles, current clinical status and future directions. Cancers (Basel). 2017;9(2):19.
15. Domka W, Bartusik-Aebisher D, Rudy I, Dynarowicz K, Pięta K, Aebisher D. Photodynamic therapy in brain cancer: mechanisms, clinical and preclinical studies and therapeutic challenges. Front Chem. 2023;11:1250621.
16. Bartusik-Aebisher D, Serafin I, Dynarowicz K, Aebisher D. Photodynamic therapy and associated targeting methods for treatment of brain cancer. Front Pharmacol. 2023;14:1250699.
17. Hsia T, Small JL, Yekula A, Batool SM, Escobedo AK, Ekanayake E, et al. Syst Rev Photodynamic Therapy Gliomas Cancers (Basel). 2023;15(15):3918.

18. Bhanja D, Wilding H, Baroz A, Trifoi M, Shenoy G, Slagle-Webb B, et al. Photodynamic therapy for glioblastoma: illuminating the path toward clinical applicability. Cancers (Basel). 2023;15(13):3427.
19. Cramer SW, Chen CC. Photodynamic therapy for the treatment of glioblastoma. Frontiers in surgery. Front Surg. 2020;6:81.
20. Ferrés A, Di Somma A, Mosteiro A, Topczewski TE, Roldán P, Pedrosa L, et al. Photodynamic therapy in glioblastoma: detection of intraoperative inadvertent 5-ALA mediated photodynamic therapeutical effect after gross total resection. Front Oncol. 2022;12:1080685.
21. Dupont C, Vermandel M, Leroy HA, Quidet M, Lecomte F, Delhem N, et al. INtraoperative photodynamic therapy for glioblastomas (INDYGO): study protocol for a phase I clinical trial. Neurosurgery. 2019;84(6):E414–9.
22. Foglar M, Aumiller M, Bochmann K, Buchner A, El Fahim M, Quach S, et al. Interstitial photodynamic therapy of glioblastomas: A Long-Term Follow-up analysis of survival and volumetric MRI data. Cancers (Basel). 2023;15(9):2603.
23. Miretti M, González Graglia MA, Suárez AI, Prucca CG. Photodynamic therapy for glioblastoma: A light at the end of the tunnel. J Photochem Photobiol. 2023;13:100161.
24. Liguori GL. Challenges and promise for glioblastoma treatment through extracellular vesicle inquiry. Cells. 2024;13(4):336.
25. Wei C, Li X. The role of photoactivated and Non-Photoactivated verteporfin on tumor. Front Pharmacol. 2020;11:557429.
26. Piorecka K, Kurjata J, Stanczyk WA. Acriflavine, an acridine derivative for biomedical application: current state of the Art. J Med Chem. 2022;65(17):11415–32.
27. Wang GL, Jiang BH, Rue EA, Semenza GL. Hypoxia-inducible factor 1 is a basic-helix-loop-helix-PAS heterodimer regulated by cellular O2 tension. Proc Natl Acad Sci U S A. 1995;92(12):5510–4.
28. Iyer NV, Kotch LE, Agani F, Leung SW, Laughner E, Wenger RH, et al. Cellular and developmental control of O2 homeostasis by hypoxia-inducible factor 1 alpha. Genes Dev. 1998;12(2):149–62.
29. Simon MC. The hypoxia response Pathways - Hats off! N Engl J Med. 2016;375(17):1687–9.
30. Bhat K, Bhat K, Tang T. DNAR-05. A ROLE FOR TAZ/YAP IN DNA DAMAGE REPAIR IN GLIOBLASTOMA. Neurooncology. 2022;24(Supplement7):vii91–vii.
31. Pefani DE, O'Neill E. Hippo pathway and protection of genome stability in response to DNA damage. FEBS J. 2016;283(8):1392–403.
32. Tan K, Feizi H, Luo C, Fan SH, Ravasi T, Ideker TG. A systems approach to delineate functions of paralogous transcription factors: role of the Yap family in the DNA damage response. Proc Natl Acad Sci U S A. 2008;105(8):2934–9.
33. Chang H-A, Ou Yang R-Z, Su J-M, Nguyen TMH, Sung J-M, Tang M-J, et al. YAP nuclear translocation induced by HIF-1α prevents DNA damage under hypoxic conditions. Cell Death Discov. 2023;9(1):385.
34. Wozny A-S, Gauthier A, Alphonse G, Malésys C, Varoclier V, Beuve M, et al. Involvement of HIF-1α in the detection, signaling, and repair of DNA Double-Strand breaks after photon and Carbon-Ion irradiation. Cancers (Basel). 2021;13(15):3833.
35. Rezaeian AH, Wang YH, Lin HK. DNA damage players are linked to HIF-1α/hypoxia signaling. Cell Cycle. 2017;16(8):725–6.
36. Broekgaarden M, Weijer R, van Gulik TM, Hamblin MR, Heger M. Tumor cell survival pathways activated by photodynamic therapy: a molecular basis for Pharmacological Inhibition strategies. Cancer Metastasis Rev. 2015;34(4):643–90.
37. Xu HZ, Li TF, Ma Y, Li K, Zhang Q, Xu YH, et al. Targeted photodynamic therapy of glioblastoma mediated by platelets with photo-controlled release property. Biomaterials. 2022;290:121833.
38. Morice S, Mullard M, Brion R, Dupuy M, Renault S, Tesfaye R, et al. The YAP/TEAD Axis as a new therapeutic target in osteosarcoma: effect of verteporfin and CA3 on primary tumor growth. Cancers (Basel). 2020;12(12):3847.
39. Wang C, Zhu X, Feng W, Yu Y, Jeong K, Guo W, et al. Verteporfin inhibits YAP function through up-regulating 14-3-3σ sequestering YAP in the cytoplasm. Am J Cancer Res. 2016;6(1):27–37.
40. Yuan Y, Hilliard G, Ferguson T, Millhorn DE. Cobalt inhibits the interaction between hypoxia-inducible factor-alpha and von Hippel-Lindau protein by direct binding to hypoxia-inducible factor-alpha. J Biol Chem. 2003;278(18):15911–6.
41. Meng Z, Moroishi T, Guan KL. Mechanisms of Hippo pathway regulation. Genes Dev. 2016;30(1):1–17.
42. Song H, Qiu Z, Wang Y, Xi C, Zhang G, Sun Z, et al. HIF-1α/YAP signaling rewrites glucose/iodine metabolism program to promote papillary thyroid Cancer progression. Int J Biol Sci. 2023;19(1):225–41.
43. Zhu B, Pan S, Liu J, Wang S, Ni Y, Xiao L, et al. HIF-1α forms regulatory loop with YAP to coordinate hypoxia-induced adriamycin resistance in acute myeloid leukemia cells. Cell Biol Int. 2020;44(2):456–66.
44. Blackford AN, Jackson SP, ATM, ATR. The trinity at the heart of the DNA damage response. Mol Cell. 2017;66(6):801–17.
45. Maréchal A, Zou L. DNA damage sensing by the ATM and ATR kinases. Cold Spring Harb Perspect Biol. 2013;5(9):a012716.
46. Raja S, Van Houten B. The multiple cellular roles of SMUG1 in genome maintenance and Cancer. Int J Mol Sci. 2021;22(4):1981.
47. Robins P, Lindahl T. DNA ligase IV from HeLa cell nuclei. J Biol Chem. 1996;271(39):24257–61.
48. Holinstat M. Normal platelet function. Cancer Metastasis Rev. 2017;36(2):195–8.
49. Puricelli C, Boggio E, Gigliotti CL, Stoppa I, Sutti S, Giordano M, et al. Platelets, protean cells with All-Around functions and multifaceted Pharmacological applications. Int J Mol Sci. 2023;24(5):4565.
50. Morimoto T, Ogihara S, Takisawa H. Anchorage of secretion-competent dense granules on the plasma membrane of bovine platelets in the absence of secretory stimulation. J Cell Biol. 1990;111(1):79–86.
51. Deranleau DA, Lüthy R, Lüscher EF. Stochastic response of human blood platelets to stimulation of shape changes and secretion. Proc Natl Acad Sci U S A. 1986;83(7):2076–80.
52. Eriksson I, Vainikka L, Persson HL, Öllinger K. Real-Time monitoring of lysosomal membrane permeabilization using acridine orange. Methods Protoc. 2023;6(4):72.
53. Sharda A, Flaumenhaft R. The life cycle of platelet granules. F1000Res. 2018;7:236.
54. Senge MO, Radomski MW. Platelets, photosensitizers, and PDT. Photodiagnosis Photodyn Ther. 2013;10(1):1–16.
55. Sharma A, Sinha S, Shrivastava N. Therapeutic targeting Hypoxia-Inducible factor (HIF-1) in cancer: cutting gordian knot of Cancer cell metabolism. Front Genet. 2022;13:849040.
56. Infantino V, Santarsiero A, Convertini P, Todisco S, Iacobazzi V. Cancer cell metabolism in hypoxia: role of HIF-1 as key regulator and therapeutic target. Int J Mol Sci. 2021;22(11):5703.
57. Wicks EE, Semenza GL. Hypoxia-inducible factors: cancer progression and clinical translation. J Clin Invest. 2022;132(11):e159839.
58. Zhang Y, Wang S, Hu H, Li X. A systematic study of HIF1A cofactors in hypoxic cancer cells. Sci Rep. 2022;12(1):18962.
59. Luo J, Deng L, Zou H, Guo Y, Tong T, Huang M, et al. New insights into the ambivalent role of YAP/TAZ in human cancers. J Exp Clin Cancer Res. 2023;42(1):130.
60. Barbosa IAM, Gopalakrishnan R, Mercan S, Mourikis TP, Martin T, Wengert S, et al. Cancer lineage-specific regulation of YAP responsive elements revealed through large-scale functional epigenomic screens. Nat Commun. 2023;14(1):3907.
61. Piccolo S, Panciera T, Contessotto P, Cordenonsi M. YAP/TAZ as master regulators in cancer: modulation, function and therapeutic approaches. Nat Cancer. 2023;4(1):9–26.
62. Liu H, Du S, Lei T, Wang H, He X, Tong R, et al. Multifaceted regulation and functions of YAP/TAZ in tumors (Review). Oncol Rep. 2018;40(1):16–28.
63. Wang S, Lu Y, Yin MX, Wang C, Wu W, Li J, et al. Importin A1 mediates yorkie nuclear import via an N-terminal Non-canonical nuclear localization signal. J Biol Chem. 2016;291(15):7926–37.
64. Wei C, Li X. Verteporfin inhibits cell proliferation and induces apoptosis in different subtypes of breast cancer cell lines without light activation. BMC Cancer. 2020;20(1):1042.
65. Li H, Li X, Jing X, Li M, Ren Y, Chen J, et al. Hypoxia promotes maintenance of the chondrogenic phenotype in rat growth plate chondrocytes through the HIF-1α/YAP signaling pathway. Int J Mol Med. 2018;42(6):3181–92.
66. Kachynski AV, Pliss A, Kuzmin AN, Ohulchanskyy TY, Baev A, Qu J, et al. Photodynamic therapy by in situ nonlinear photon conversion. Nat Photonics. 2014;8(6):455–61.
67. Zhao PD, Chen P, Tang GQ, Zhang GL, Chen WJ. Two-photon spectroscopic properties of a new Chlorin derivative photosensitizer. Chem Phys Lett. 2004;390(1):41–4.
68. Gattuso H, Monari A, Marazzi M. Photophysics of Chlorin e6: from one- and two-photon absorption to fluorescence and phosphorescence. RSC Adv. 2017;7(18):10992–9.
69. Wang M-F, Guo J, Yuan S-J, Li K, Zhang Q, Lei H-M, et al. Targeted sonodynamic therapy induces tumor cell quasi-immunogenic ferroptosis and

macrophage immunostimulatory autophagy in glioblastoma. Biomaterials. 2025;315:122913.
70. Wang M, Xu H, Li T, Li K, Zhang Q, Chen S, et al. Sonodynamic therapy of glioblastoma mediated by platelets with ultrasound-triggered drug release. Drug Delivery. 2023;30(1):2219429.
71. Quach S, Schwartz C, Aumiller M, Foglar M, Schmutzer M, Katzendobler S, et al. Interstitial photodynamic therapy for newly diagnosed glioblastoma. J Neurooncol. 2023;162(1):217–23.
72. Leroy HA, Guérin L, Lecomte F, Baert G, Vignion AS, Mordon S, et al. Is interstitial photodynamic therapy for brain tumors ready for clinical practice? A systematic review. Photodiagnosis Photodyn Ther. 2021;36:102492.
73. Ozawa T, James CD. Establishing intracranial brain tumor xenografts with subsequent analysis of tumor growth and response to therapy using bioluminescence imaging. J Visualized Exp. 2010;41:1986.

## Publisher's note